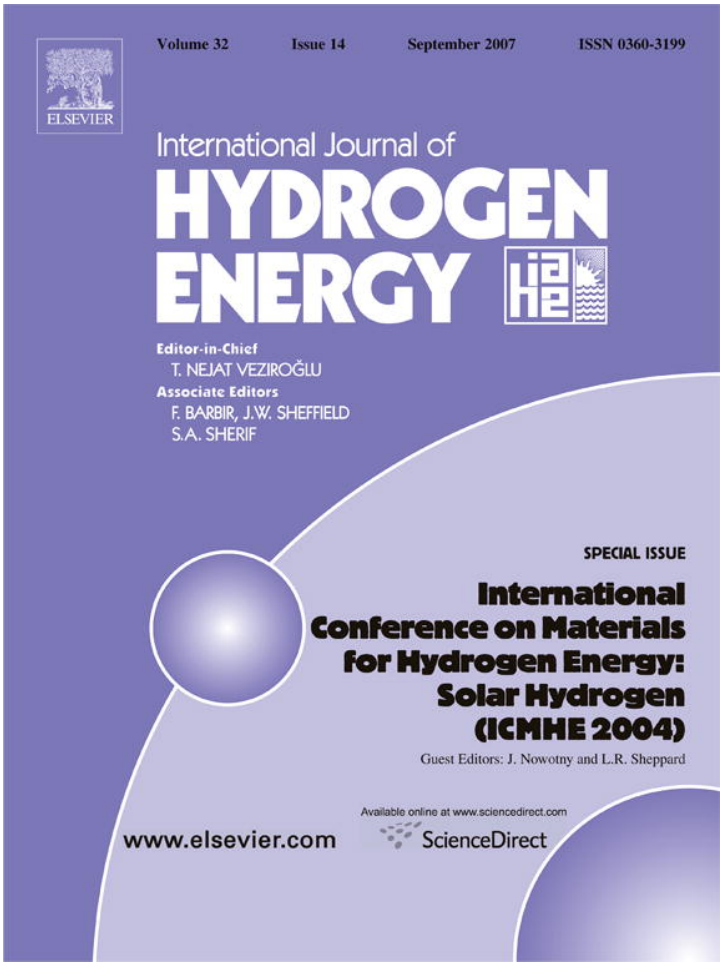

Available online at www.sciencedirect.com
ScienceDirect
International Journal of Hydrogen Energy 32 (2007) 2988–3009
International Journal of HYDROGEN ENERGY
www.elsevier.com/locate/ijhydene

Comprehensive identification and potential applications of new states of hydrogen

Randell L. Mills*, Jiliang He, Ying Lu, Mark Nansteel, Zhixiang Chang, Bala Dhandapani

BlackLight Power, Inc., 493 Old Trenton Road, Cranbury, NJ 08512, USA

Received 30 March 2007; accepted 31 March 2007
Available online 25 May 2007

Abstract

The data from a broad spectrum of investigational techniques strongly and consistently indicate that hydrogen can exist in lower-energy states then previously thought possible. Novel emission lines with energies of $q \cdot 13.6\,\text{eV}$ where $q = 1, 2, 3, 4, 6, 7, 8, 9, 11$ were previously observed by extreme ultraviolet (EUV) spectroscopy recorded on microwave discharges of helium with 2% hydrogen [Mills RL, Ray P. Extreme ultraviolet spectroscopy of helium-hydrogen plasma. J Phys D 2003;36:1535–42]. These lines matched $H(1/p)$, fractional Rydberg states of atomic hydrogen wherein $n = \frac{1}{2}, \frac{1}{3}, \frac{1}{4}, \ldots, \frac{1}{p}$; ($p \leqslant 137$ is an integer) replaces the well-known parameter $n =$ integer in the Rydberg equation for hydrogen excited states. Evidence supports that these states are formed by a resonant nonradiative energy transfer to He^+ acting as a catalyst. Ar^+ and K also serve as catalysts since, like He^+, they meet the catalyst criterion—a chemical or physical process with an enthalpy change equal to an integer multiple of the potential energy of atomic hydrogen, 27.2 eV.

Two $H(1/p)$ may react to form $H_2(1/p)$ that have vibrational and rotational energies that are p^2 times those of H_2 comprising uncatalyzed atomic hydrogen. Rotational lines were observed in the 145–300 nm region from atmospheric pressure electron-beam excited argon–hydrogen plasmas. The unprecedented energy spacing of 4^2 times that of hydrogen established the internuclear distance as $\frac{1}{4}$ that of H_2 and identified $H_2(\frac{1}{4})$. The predicted products of alkali catalyst K are $H^-(\frac{1}{4})$ which form a novel alkali halido hydride compound (MH*X) and $H_2(\frac{1}{4})$ which may be trapped in the crystal. The ^{1}H MAS NMR spectrum of novel compound KH*Cl relative to external tetramethylsilane (TMS) showed a large distinct upfield resonance at −4.4 ppm corresponding to an absolute resonance shift of −35.9 ppm that matched the theoretical prediction of $H^-(1/p)$ with $p = 4$. The predicted catalyst reactions, position of the upfield-shifted NMR peaks for $H^-(\frac{1}{4})$, and spectroscopic data for $H^-(\frac{1}{4})$ were found to be in agreement with the experimental observations as well as previously reported analysis of KH*Cl containing this hydride ion.

The predicted frequencies of ortho- and para-$H_2(\frac{1}{4})$ were observed at 1943 and 2012 cm^{-1} in the high resolution FTIR spectrum of KH*I having a −4.6 ppm NMR peak assigned to $H^-(\frac{1}{4})$. The 1943/2012 cm^{-1}-intensity ratio matched the characteristic ortho-to-para-peak-intensity ratio of 3:1, and the ortho–para splitting of 69 cm^{-1} matched that predicted. KH*Cl having $H^-(\frac{1}{4})$ by NMR was incident to the 12.5 keV electron-beam which excited similar emission of interstitial $H_2(\frac{1}{4})$ as observed in the argon–hydrogen plasma. $H_2(1/p)$ gas was isolated by liquefaction of plasma gas at liquid nitrogen temperature and by decomposition of compounds (MH*X) found to contain the corresponding hydride ions $H^-(1/p)$. The $H_2(1/p)$ gas was dissolved in $CDCl_3$ and characterized by ^{1}H NMR. Considering solvent effects, singlet peaks upfield of H_2 were observed with a predicted integer spacing of 0.64 ppm at 3.47, 3.02, 2.18, 1.25, 0.85, and 0.22 ppm which matched the consecutive series $H_2(\frac{1}{2})$, $H_2(\frac{1}{3})$, $H_2(\frac{1}{4})$, $H_2(\frac{1}{5})$, $H_2(\frac{1}{6})$, and $H_2(\frac{1}{7})$, respectively.

Excess power was absolutely measured from the helium–hydrogen plasma. For an input of 41.9 W, the total plasma power of the helium–hydrogen plasma measured by water bath calorimetry was 62.1 W corresponding to 20.2 W of excess power in 3 cm^3 plasma volume. The excess power density and energy balance were high, 6.7 W/cm^3 and -5.4×10^4 kJ/mole H_2 (280 eV/H atom), respectively. In addition to power applications, battery and propellant reactions are proposed that may be transformational, and observed excited vibration–rotational levels of $H_2(\frac{1}{4})$ could be the basis of a UV laser that could significantly advance photolithography.

Keywords: Fractional-principal-quantum-level atomic and molecular hydrogen; Vibrational series; Rotational series; LN-condensable hydrogen; NMR series; Exothermic plasma catalysis reaction; Applications

* Corresponding author. Tel.: +1 609 490 1090; fax: +1 609 490 1066.
E-mail address: rmills@blacklightpower.com (R.L. Mills).

0360-3199/$ - see front matter © 2007 International Association for Hydrogen Energy. Published by Elsevier Ltd. All rights reserved.
doi:10.1016/j.ijhydene.2007.03.035

1. Introduction

1.1. Theoretical predictions

The basic spectral emission of pure helium and hydrogen light sources have been well known for about a century. Recently, however, unique vacuum ultraviolet (VUV) emission lines were found at predicted wavelengths and reported in numerous publications [1–3]. For example, extreme ultraviolet (EUV) spectroscopy was recorded on microwave discharges of helium with 2% hydrogen. Novel emission lines were observed with energies of $q \cdot 13.6\,\text{eV}$, $q = 1, 2, 3, 7, 9, 11$ or $q \cdot 13.6\,\text{eV}$, $q = 4, 6, 8$ less 21.2 eV corresponding to inelastic scattering of these photons by helium atoms due to excitation of $\text{He}(1s^2)$ to $\text{He}(1s^1 2p^1)$. These strong emissions are not found in any single gas plasma, and cannot be assigned to the known emission of any species of the single gases studied such as H, H^-, H_2, H_2^+, H_3^+, He, He_2^* and He^+, known species of the mixture such as He_2^+, HeH^+, HeH, HHe_2^+, and HHe_n^+ and He_n, possible contaminants [1], or doubly excited states [4]. However, the results can be explained by a novel catalytic reaction involving atomic hydrogen [1–3].

J.R. Rydberg showed that all of the spectral lines of atomic hydrogen were given by a completely empirical relationship

$$\bar{v} = R\left(\frac{1}{n_f^2} - \frac{1}{n_i^2}\right), \tag{1}$$

where $R = 109,677\,\text{cm}^{-1}$, $n_f = 1, 2, 3, \ldots$, $n_i = 2, 3, 4, \ldots$ and $n_i > n_f$. Bohr, Schrödinger, and Heisenberg each developed a theory for atomic hydrogen that gave the energy levels in agreement with Rydberg's equation.

$$E_n = -\frac{e^2}{n^2 8\pi\varepsilon_0 a_\text{H}} = -\frac{13.598\,\text{eV}}{n^2}, \tag{2a}$$

$$n = 1, 2, 3, \ldots, \tag{2b}$$

where e is the elementary charge, ε_0 is the permittivity of vacuum, and a_H is the radius of the hydrogen atom. The excited energy states of atomic hydrogen are given by Eq. (2a) for $n > 1$ in Eq. (2b). The $n = 1$ state is the "ground" state for "pure" photon transitions (i.e. the $n = 1$ state can absorb a photon and go to an excited electronic state, but it cannot release a photon and go to a lower-energy electronic state). However, an electron transition from the ground state to a lower-energy state may be possible by a resonant nonradiative energy transfer such as multipole coupling or a resonant collision mechanism. Processes such as hydrogen molecular bond formation that occur without photons and that require collisions are common [5]. Also, some commercial phosphors are based on resonant nonradiative energy transfer involving multipole coupling [6].

The theory reported previously [1–3,7–17] predicts that atomic hydrogen may undergo a catalytic reaction with certain atoms, excimers, and ions which provide a reaction with a net enthalpy of an integer multiple of the potential energy of atomic hydrogen, $E_\text{h} = 27.2\,\text{eV}$ where E_h is one hartree. Specific species (e.g. He^+, Ar^+, and K) identifiable on the basis of their known electron energy levels are required to be present in plasmas with atomic hydrogen to catalyze the process. In contrast, species such as atoms or ions of Kr or Xe do not fulfill the catalyst criterion—a chemical or physical process with an enthalpy change equal to an integer multiple of E_h that is sufficiently reactive with atomic hydrogen under reaction conditions. The reaction involves a nonradiative energy transfer followed by $q \cdot 13.6\,\text{eV}$ emission or $q \cdot 13.6\,\text{eV}$ transfer to H to form extraordinarily hot, excited-state H [10–21] and a hydrogen atom that is lower in energy than unreacted atomic hydrogen that corresponds to a fractional principal quantum number. That is

$$n = \frac{1}{2}, \frac{1}{3}, \frac{1}{4}, \ldots, \frac{1}{p}; \quad p \leqslant 137 \text{ is an integer} \tag{2c}$$

replaces the well-known parameter $n =$ integer in the Rydberg equation for hydrogen excited states. The $n = 1$ state of hydrogen and the $n = 1/\text{integer}$ states of hydrogen are nonradiative, but a transition between two nonradiative states, say $n = 1$ to $\frac{1}{2}$, is possible via a nonradiative energy transfer. Thus, a catalyst provides a net positive enthalpy of reaction of $m \cdot 27.2\,\text{eV}$ (i.e. it resonantly accepts the nonradiative energy transfer from hydrogen atoms and releases the energy to the surroundings to affect electronic transitions to fractional quantum energy levels). As a consequence of the nonradiative energy transfer, the hydrogen atom becomes unstable and emits further energy until it achieves a lower-energy nonradiative state having a principal energy level given by Eqs. (2a) and (2c).

Prior related studies that support the possibility of a novel reaction of atomic hydrogen which produces hydrogen in fractional quantum states that are at lower energies than the traditional "ground" ($n = 1$) state include extreme ultraviolet (EUV) spectroscopy [1–3,9–14,16,19,21–25,28–30], characteristic emission from catalysts and the hydride ion products [11–13,21–25], lower-energy hydrogen emission [1–3,28–30], chemically formed plasmas [9–16,21–25], Balmer α line broadening [1,2,10–13,15–21,24,25,28,30], population inversion of H lines [13,21,24–26], elevated electron temperature [1,2,17–19,28], anomalous plasma afterglow duration [13,14], power generation [2,13,15,19,27–30], and analysis of novel chemical compounds [13,29,31–33].

$H(1/p)$ may react with a proton and two $H(1/p)$ may react to form $H_2(1/p)^+$ and $H_2(1/p)$, respectively. The hydrogen molecular ion and molecular charge and current density functions, bond distances, and energies were solved previously [7,8] from the Laplacian in ellipsoidal coordinates with the constraint of nonradiation.

$$(\eta - \zeta)R_\xi \frac{\partial}{\partial \xi}\left(R_\xi \frac{\partial \phi}{\partial \xi}\right) + (\zeta - \xi)R_\eta \frac{\partial}{\partial \eta}\left(R_\eta \frac{\partial \phi}{\partial \eta}\right) + (\xi - \eta)R_\zeta \frac{\partial}{\partial \zeta}\left(R_\zeta \frac{\partial \phi}{\partial \zeta}\right) = 0. \tag{3}$$

The total energy of the hydrogen molecular ion having a central field of $+pe$ at each focus of the prolate spheroid molecular

orbital is

$$E_T = -p^2\left\{\frac{e^2}{8\pi\varepsilon_0 a_H}(4\ln 3 - 1 - 2\ln 3)\right.$$
$$\left.\times\left[1 + p\sqrt{\frac{2\hbar\sqrt{\dfrac{2e^2}{4\pi\varepsilon_0(2a_H)^3}}{m_e}}{m_e c^2}} - \frac{1}{2}\hbar\sqrt{\frac{k}{\mu}}\right]\right\}$$
$$= -p^2 16.13392\,\text{eV} - p^3 0.118755\,\text{eV}, \quad (4)$$

where p is an integer, $\hbar$ is Planck's constant bar, m_e is the mass of the electron, c is the speed of light in vacuum, μ is the reduced nuclear mass, and k is the harmonic force constant solved previously in a closed-form equation with fundamental constants only [7,8]. The total energy of the hydrogen molecule having a central field of $+pe$ at each focus of the prolate spheroid molecular orbital is

$$E_T = -p^2\left\{\frac{e^2}{8\pi\varepsilon_0 a_0}\left[\left(2\sqrt{2} - \sqrt{2} + \frac{\sqrt{2}}{2}\right)\ln\frac{\sqrt{2}+1}{\sqrt{2}-1} - \sqrt{2}\right]\right.$$
$$\left.\times\left[1 + p\sqrt{\frac{2\hbar\sqrt{\dfrac{e^2}{4\pi\varepsilon_0 a_0^3}}{m_e}}{m_e c^2}} - \frac{1}{2}\hbar\sqrt{\frac{k}{\mu}}\right]\right\}$$
$$= -p^2 31.351\,\text{eV} - p^3 0.326469\,\text{eV}, \quad (5)$$

where a_0 is the Bohr radius.

The bond dissociation energy, E_D, of hydrogen molecule $H_2(1/p)$ is the difference between the total energy of the corresponding hydrogen atoms and E_T

$$E_D = E(2H(1/p)) - E_T, \quad (6)$$

where [34]

$$E(2H(1/p)) = -p^2 27.20\,\text{eV}. \quad (7)$$

E_D is given by Eqs. (6)–(7) and (5):

$$E_D = -p^2 27.20\,\text{eV} - E_T$$
$$= -p^2 27.20\,\text{eV} - (-p^2 31.351\,\text{eV} - p^3 0.326469\,\text{eV})$$
$$= p^2 4.151\,\text{eV} + p^3 0.326469\,\text{eV}. \quad (8)$$

The calculated and experimental parameters of H_2, D_2, H_2^+, and D_2^+ from Refs. [7,8] are given in Table 1.

The vibrational energies, E_{vib}, for the $\upsilon = 0$–1 transition of hydrogen-type molecules $H_2(1/p)$ are [7,8]

$$E_{vib} = p^2 0.515902\,\text{eV}, \quad (9)$$

where p is an integer and the experimental vibrational energy for the $\upsilon = 0$–1 transition of H_2, $E_{H_2(\upsilon=0\to\upsilon=1)}$, is given by Beutler [35] and Herzberg [36].

The rotational energies, E_{rot}, for the J to $J+1$ transition of hydrogen-type molecules $H_2(1/p)$ are [7,8]

$$E_{rot} = E_{J+1} - E_J = \frac{\hbar^2}{I}[J+1]$$
$$= p^2(J+1)0.01509\,\text{eV}, \quad (10)$$

where p is an integer, I is the moment of inertia, and the experimental rotational energy for the $J = 0$–1 transition of H_2 is given by Atkins [37].

The p^2 dependence of the rotational energies results from an inverse p dependence of the internuclear distance and the corresponding impact on I. The predicted internuclear distance $2c'$ for $H_2(1/p)$ is

$$2c' = \frac{a_0\sqrt{2}}{p}. \quad (11)$$

1.2. Experiments to test the theoretical predictions

The reaction Ar^+ to Ar^{2+} has a net enthalpy of reaction of 27.63 eV; thus, it may serve as a catalyst to form $H(\frac{1}{2})$. The product of the catalysis reaction, $H(\frac{1}{2})$, may further serve as both a catalyst and a reactant to form $H(\frac{1}{4})$ [2,3]. Also, the second ionization energy of helium is 54.4 eV; thus, the ionization reaction of He^+ to He^{2+} has a net enthalpy of reaction of 54.4 eV which is equivalent to $2 \cdot 27.2$ eV. The product of the catalysis reaction, $H(\frac{1}{3})$, may further serve as both a catalyst and a reactant to form $H(\frac{1}{4})$ and $H(\frac{1}{2})$ [2,3].

The present paper tests theoretical predictions [1–3,7,8] that atomic and molecular hydrogen form stable states of lower energy than traditionally thought possible. Substantial spectroscopic and physical differences are anticipated. For example, novel EUV atomic and molecular spectral emission lines from transitions corresponding to energy levels given by Eqs. (2a) and (2c) and Eq. (5), respectively, are predicted. The atomic lines have been shown previously [1–3]. To test additional predictions, EUV spectroscopy was performed to search for emission that was characteristic of and identified $H_2(\frac{1}{4})$. Closed-form solutions of the parameters hydrogen molecules are available for testing [7,8].

The rotational energies provide a very precise measure of I and the internuclear distance using well established theory [38].

Table 1
The Maxwellian closed-form calculated and experimental parameters of H_2, D_2, H_2^+ and D_2^+

Parameter	Calculated	Experimental	Eqs.[a]
H_2 Bond energy	4.478 eV	4.478 eV	261
D_2 Bond energy	4.556 eV	4.556 eV	263
H_2^+ Bond energy	2.654 eV	2.651 eV	230
D_2^+ Bond energy	2.696 eV	2.691 eV	232
H_2 Total energy	31.677 eV	31.675 eV	257
D_2 Total energy	31.760 eV	31.760 eV	258
H_2 Ionization energy	15.425 eV	15.426 eV	259
D_2 Ionization energy	15.463 eV	15.466 eV	260
H_2^+ Ionization energy	16.253 eV	16.250 eV	228
D_2^+ Ionization energy	16.299 eV	16.294 eV	229
H_2^+ Magnetic moment	9.274×10^{-24} JT^{-1} μ_B	9.274×10^{-24} JT^{-1} μ_B	328–334
Absolute H_2 Gas-Phase NMR Shift	−28.0 ppm	−28.0 ppm	345
H_2 Internuclear distance[b]	0.748 Å $\sqrt{2}a_0$	0.741 Å	248
D_2 Internuclear distance[b]	0.748 Å $\sqrt{2}a_0$	0.741 Å	248
H_2^+ Internuclear distance	1.058 Å $2a_0$	1.06 Å	217
D_2^+ Internuclear distance[b]	1.058 Å $2a_0$	1.0559 Å	217
H_2 Vibrational energy	0.517 eV	0.516 eV	269
D_2 Vibrational energy	0.371 eV	0.371 eV	274
H_2 $\omega_e x_e$	120.4 cm^{-1}	121.33 cm^{-1}	271
D_2 $\omega_e x_e$	60.93 cm^{-1}	61.82 cm^{-1}	275
H_2^+ Vibrational energy	0.270 eV	0.271 eV	238
D_2^+ Vibrational energy	0.193 eV	0.196 eV	242
H_2 $J = 1$–0 rotational energy[b]	0.0148 eV	0.01509 eV	290
D_2 $J = 1$–0 rotational energy[b]	0.00741 eV	0.00755 eV	278–283, 290
H_2^+ $J = 1$–0 rotational energy	0.00740 eV	0.00739 eV	286
D_2^+ $J = 1$–0 rotational energy[b]	0.00370 eV	0.003723 eV	278–286

[a]Ref. [8].
[b]Not corrected for the slight reduction in internuclear distance due to $\overline{E}_{osc}$.

Neutral molecular emission was anticipated for high pressure argon–hydrogen plasmas excited by a 12.5 keV electron beam. Rotational lines for $H_2(\frac{1}{4})$ were anticipated and sought in the 150–250 nm region. The spectral lines were compared to those predicted by Eqs. (9)–(10) corresponding to the internuclear distance of $\frac{1}{4}$ that of H_2 given by Eq. (11). The predicted energies for the $\upsilon = 1 \rightarrow \upsilon = 0$ vibration–rotational series of $H_2(\frac{1}{4})$ (Eqs. (9)–(10)) are

$$\begin{aligned} E_{\text{vib–rot}} &= p^2 E_{\text{vib H}_2(\upsilon=0\rightarrow\upsilon=1)} \pm p^2(J+1)E_{\text{rot H}_2} \\ &= 4^2 E_{\text{vib H}_2(\upsilon=0\rightarrow\upsilon=1)} \pm 4^2(J+1)E_{\text{rot H}_2} \quad J = 0, 1, 2, 3 \ldots \\ &= 8.254432\,\text{eV} \pm (J+1)0.24144\,\text{eV}, \end{aligned} \tag{12}$$

for $p = 4$. The catalyst reaction of Ar^+ to Ar^{2+} forms $H(\frac{1}{2})$ which may further serve as both a catalyst and a reactant to form $H(\frac{1}{4})$ [2,3]; thus, the observation of $H(\frac{1}{4})$ is predicted to be flow dependent since the formation of $H_2(\frac{1}{4})$ requires the buildup of intermediates. The mechanism was tested by experiments with flowing plasma gases.

Selection rules based on nuclear-spin rotational coupling are common [39–46]. It is proposed that the vibration–rotational transitions of $H_2(\frac{1}{4})$ are allowed with nuclear spin–rotational coupling. The nuclear spin quantum number for the proton is $I = \frac{1}{2}$, and the selection rule for nuclear spin transitions are $\Delta I = \pm 1$. These transitions can couple to the rotational quantum states such that the P-branch transitions with $\Delta J = 1$ are allowed since the nuclear–rotational interaction is of the form $-\hbar C \mathbf{I}_k \cdot \mathbf{J}$ [39–41] where $\mathbf{I}_k$ is the spin of the nucleus k, $\mathbf{J}$ is the rotational angular momentum, C is the spin–rotational constant, and $\Delta I = 1$ to conserve angular momentum that is quantized in terms of units of $\hbar$. In addition, the transition corresponding to $R(0)$ is allowed since the corresponding final state does not rotate and has a relative infinite half-life. Thus, the vibrational rotational spectrum of $H_2(\frac{1}{4})$ is predicted to comprise only the $R(0)$ line and the P branch.

The product $H_2(1/p)$ gas was isolated by liquefaction at liquid nitrogen temperature. The boiling point of the novel molecular hydrogen product is predicted to be different from that of H_2. The ℓ quantum number of $H_2(1/p)$ may be different from zero [7,8] which would give rise to a dipole moment with a corresponding significant increase in the liquefaction temperature relative to H_2 with no dipole moment. Helium–hydrogen (90%/10%) plasma gases were flowed through a high-vacuum (10^{-6} Torr) capable, liquid nitrogen (LN) cryotrap, and the condensed gas was characterized by ^{1}H nuclear magnetic resonance (NMR) of the LN-condensable gas dissolved in $CDCl_3$. Other

sources of hydrogen such as hydrocarbons were eliminated by mass spectroscopy (MS) and Fourier transform infrared spectroscopy (FTIR). The ^{1}H NMR resonance of $H_2(1/p)$ is predicted to be upfield from that of H_2 due to the fractional dimensions in elliptic coordinates [7,8] wherein the electrons are significantly closer to the nuclei. The predicted shift, $\frac{\Delta B_T}{B}$, for $H_2(1/p)$ derived previously [7,8] is given by the sum of that of H_2 and a relativistic term that depends on $p > 1$:

$$\frac{\Delta B_T}{B} = -\mu_0 \left(4 - \sqrt{2} \ln \frac{\sqrt{2}+1}{\sqrt{2}-1}\right) \frac{e^2}{36 a_0 m_e} (1 + \pi\alpha p), \quad (13)$$

$$\frac{\Delta B_T}{B} = -(28.01 + 0.64p)\,\text{ppm}, \quad (14)$$

where for H_2 there is no relativistic effect and $p = \text{integer} > 1$ for $H_2(1/p)$.

The catalyst product, $H(1/p)$, may also react with an electron to form a novel hydride ion $H^-(1/p)$ with a binding energy E_B [7,9,21]:

$$E_B = \frac{\hbar^2 \sqrt{s(s+1)}}{8\mu_e a_0^2 \left[\frac{1+\sqrt{s(s+1)}}{p}\right]^2} - \frac{\pi\mu_0 e^2 \hbar^2}{m_e^2} \times \left(\frac{1}{a_H^3} + \frac{2^2}{a_0^3 \left[\frac{1+\sqrt{s(s+1)}}{p}\right]^3}\right), \quad (15)$$

where p is an integer greater than one, $s = \frac{1}{2}$, $\hbar$ is Planck's constant bar, μ_0 is the permeability of vacuum, m_e is the mass of the electron, μ_e is the reduced electron mass given by $\mu_e = \frac{m_e m_p}{\frac{m_e}{\sqrt{\frac{3}{4}}} + m_p}$ where m_p is the mass of the proton, a_H is the radius of the hydrogen atom, a_0 is the Bohr radius, e is the elementary charge, and the ionic radius is $r_1 = (a_0/p)(1 + \sqrt{s(s+1)})$, $s = \frac{1}{2}$. From Eq. (15), the calculated ionization energy of the hydride ion is 0.75418 eV, and the experimental value given by Lykke [47] is $6082.99 \pm 0.15\,\text{cm}^{-1}$ (0.75418 eV).

Substantial evidence of an energetic catalytic reaction was previously reported [13] involving a resonant energy transfer between hydrogen atoms and K to form a chemically generated plasma (rt-plasma). The products are more stable hydride and molecular hydrogen species such as $H^-(\frac{1}{4})$ and $H_2(\frac{1}{4})$. In general, an rt-plasma source operates by incandescently heating a hydrogen dissociator and a catalyst to provide atomic hydrogen and gaseous catalyst, respectively, such that the catalyst reacts with the atomic hydrogen to produce a plasma. It was extraordinary that intense EUV emission was observed by Mills et al. [9–16,21–25] at low temperatures (e.g. $\approx 10^3$ K) and an extraordinary low field strength of about 1–2 V/cm from atomic hydrogen and only certain atomized elements or certain gaseous ions which singly or multiply ionize at integer multiples of the potential energy of atomic hydrogen, 27.2 eV. Characteristic emission was observed from K^{3+} that confirmed the resonant nonradiative energy transfer of $3 \cdot 27.2$ eV from atomic hydrogen to K. From Eq. (15), the binding energy E_B of $H^-(\frac{1}{4})$ is

$$E_B = 11.232\,\text{eV}\ (\lambda_{vac} = 1103.8\,\text{Å}). \quad (16)$$

The product hydride ion $H^-(\frac{1}{4})$ was observed spectroscopically at 110 nm corresponding to its predicted binding energy of 11.2 eV [7,13,21,22] which was confirmed by X-ray photoelectron spectroscopy (XPS) [29,32].

Upfield-shifted NMR peaks are a direct evidence of the existence of lower-energy state hydrogen with a reduced radius relative to ordinary hydride ion and having an increase in diamagnetic shielding of the proton. The shift was given by the sum of that of ordinary hydride ion H^- and a component due to a relativistic effect:

$$\frac{\Delta B_T}{B} = -\mu_0 \frac{e^2}{12 m_e a_0 (1+\sqrt{s(s+1)})} (1 + \alpha 2\pi p) = -(29.9 + 1.37p)\,\text{ppm}, \quad (17)$$

where for H^- there is no relativistic effect and $p = \text{integer} > 1$ for $H^-(1/p)$. Corresponding alkali hydrides and alkali hydrino hydrides (containing $H^-(1/p)$) were characterized by ^{1}H MAS NMR and compared to the theoretical values. A match of the predicted and observed peaks with no alternative represents a definite test.

The ^{1}H MAS NMR spectrum of novel compound KH*Cl relative to external tetramethylsilane (TMS) showed a large distinct upfield resonance at −4.4 ppm corresponding to an absolute resonance shift of −35.9 ppm that matched the theoretical prediction of $p = 4$ [7,13,29,31–33]. The upfield-shifted NMR peak which identified the product as $H^-(\frac{1}{4})$ confirmed the previous observations from the rt-plasmas of intense hydrogen Lyman emission, a stationary inverted Lyman population, excessive afterglow duration, highly energetic hydrogen atoms, characteristic alkali-ion emission due to catalysis, predicted novel spectral lines, and the measurement of a power beyond any conventional chemistry [13] that matched predictions for a catalytic reaction of atomic hydrogen to form more stable hydride ions designated $H^-(1/p)$. Since the comparison of theory and experimental shifts of KH*Cl is direct evidence of lower-energy hydrogen with an implicit large exotherm during its formation, the NMR results were repeated with the further analysis by infrared (FTIR) spectroscopy to eliminate any known explanation.

Elemental analysis identified [31,32] these compounds as only containing the alkaline metal, halogen, and hydrogen, and no known hydride compound of this composition could be found in the literature which has an upfield-shifted hydride NMR peak. Ordinary alkali hydrides alone or mixed with alkali halides show down-field shifted peaks [13,29,31–33]. From the literature, the list of alternatives to $H^-(1/p)$ as a possible source of the upfield NMR peaks was limited to U centered H. The intense and characteristic infrared vibration band at $503\,\text{cm}^{-1}$ due to the substitution of H^- for Cl^- in KCl [48] enabled us to study the relationship between the upfield-shifted NMR peaks and any U centered H that may somehow have caused the upfield-shifted peaks.

As a further characterization, FTIR analysis of these crystals with $H^-(\frac{1}{4})$ was performed before and after storage in argon for 90 days to search for interstitial $H_2(\frac{1}{4})$ having a predicted rotational energy given by Eq. (10). The identification of single rotational peaks at this energy with ortho–para splitting due to free rotation of a very small hydrogen molecule would represent definite proof of its existence since there is no other possible assignment.

In addition to liquefaction at liquid nitrogen temperature, $H_2(1/p)$ gas was also isolated by decomposition of compounds found to contain the corresponding hydride ions $H^-(1/p)$. The decomposition reaction of $H^-(1/p)$ is

$$2M^+H^-(1/p) \xrightarrow{\Delta} H_2(1/p) + 2M, \quad (18)$$

where M^+ is a metal ion. NMR peaks of $H_2(1/p)$ given by Eqs. (13)–(14) provide a direct test of whether compounds such as KH*I contain hydride ions in the same fractional quantum state p. Furthermore, the observation of a series of singlet peaks upfield of H_2 with a predicted integer spacing of 0.64 ppm provides a powerful means to confirm the existence of $H_2(1/p)$.

Since the rotational emission of $H_2(\frac{1}{4})$ was observed in crystals of KH*I having a peak assigned to $H^-(\frac{1}{4})$ (Section 3.1.3), $H_2(\frac{1}{4})$ was released by thermal decomposition as indicated by ^{1}H NMR, and the vibration–rotational emission of $H_2(\frac{1}{4})$ was observed from 12.5 keV-electron-beam-maintained plasmas of argon with 1% hydrogen due to collisional excitation of $H_2(\frac{1}{4})$ (Section 3.1.1), $H_2(\frac{1}{4})$ trapped in the lattice of KH*Cl was investigated by windowless EUV spectroscopy on electron-beam excitation of the crystals using the 12.5 keV electron gun at pressures below which any gas could produce detectable emission ($< 10^{-5}$ Torr). The rotational energy of $H_2(\frac{1}{4})$ was confirmed by this technique as well. Consistent results from the broad spectrum of investigational techniques provided definitive evidence that hydrogen can exist in lower-energy states then previously thought possible which identifies a new power source.

The exothermic helium plasma catalysis of atomic hydrogen was shown previously by the observation of extraordinarily hot H that had no conventional explanation [17,18,20]. Since the electronic transitions are very energetic, power balances of helium–hydrogen plasmas compared to control krypton plasmas were measured using water bath calorimetry to determine whether this reaction has sufficient kinetics to merit its consideration as a practical power source.

2. Experimental

2.1. Electron-gun plasma spectroscopy

Vibration–rotational emission of $H_2(\frac{1}{4})$ was investigated using a 12.5 keV electron gun with a beam current of 10 μA as described previously [49,50] to initiate argon plasmas with 1% hydrogen in the pressure range of 450–1000 Torr. Krypton and xenon replaced argon in the controls, and argon, hydrogen, oxygen, nitrogen, water vapor, nitrogen–oxygen (50/50%), and argon or krypton with oxygen addition up to 100% oxygen served as further controls. The Ar^+ catalyst mechanism was tested by atmospheric-pressure-plasma-gas flow at 75 sccm and nonflow conditions. The electron gun was sealed with a thin (300 nm thickness) SiN_x foil that served as a 1 mm^2 electron window to the cell at high gas pressure (760 Torr), and the light emitted by beam excitation exited the cell through a MgF_2 window mounted at the entrance of a normal incidence McPherson 0.2 m monochromator (Model 302) equipped with a 1200 lines/mm holographic grating with a platinum coating. The resolution was 0.5 nm (FWHM) at an entrance and exit slit width of 100 μm. The increment was 0.1 nm and the dwell time was 1 s. The PMT (Model R8486, Hamamatsu) used has a spectral response in the range of 115–320 nm with a peak efficiency at about 225 nm. The emission was essentially flat for $200 < \lambda > 275$ nm, but a notch in the response of about 20% existed in the short wavelength range with a minimum at 150 nm. Peak assignments were determined by an external calibration against standard line emissions.

2.2. Synthesis of KH*Cl and KH*I

Potassium iodo hydride and potassium chloro hydride (KH*Cl and KH*I) were synthesized by reaction of atomic hydrogen with potassium metal (Aldrich Chemical Company 99%) as the catalyst with the corresponding alkali halide, KCl (Alfa Aesar ACS grade 99+%) or KI (Aldrich Chemical Company 99.9%), as an additional reactant. The compounds were prepared in a stainless steel gas cell comprising a Ni screen hydrogen dissociator (Belleville Wire Cloth Co., Inc.), catalyst, and alkali halide as described previously [31,32]. The reactor was run at 650 °C in a kiln for 72 h, then cooled under helium atmosphere. The sealed reactor was then opened in a glove box having an Ar atmosphere. NMR samples were placed in glass ampules, sealed with a rubber septa, and transferred out of the chamber to be flame sealed in atmosphere.

2.3. ^{1}H MAS NMR

^{1}H MAS NMR was performed on solid samples of KH*Cl and KH*I at Spectral Data Services, Inc., Champaign, Illinois as described previously [13,31–33]. Chemical shifts were referenced to external TMS. To eliminate the possibility that the alkali halide MX influenced the local environment of the ordinary alkali hydride MH to produce an NMR resonance that was shifted upfield relative to MH alone, controls comprising MH and an equimolar MH/MX mixture were run. The reference of each novel hydride comprised the corresponding ordinary hydride MH (Aldrich Chemical Company 99%) and equivalent molar mixtures of MH and MX prepared in a glove box under argon.

2.4. FTIR spectroscopy

FTIR analysis was performed on solid-sample-KBr pellets using the transmittance mode at the Department of Chemistry,

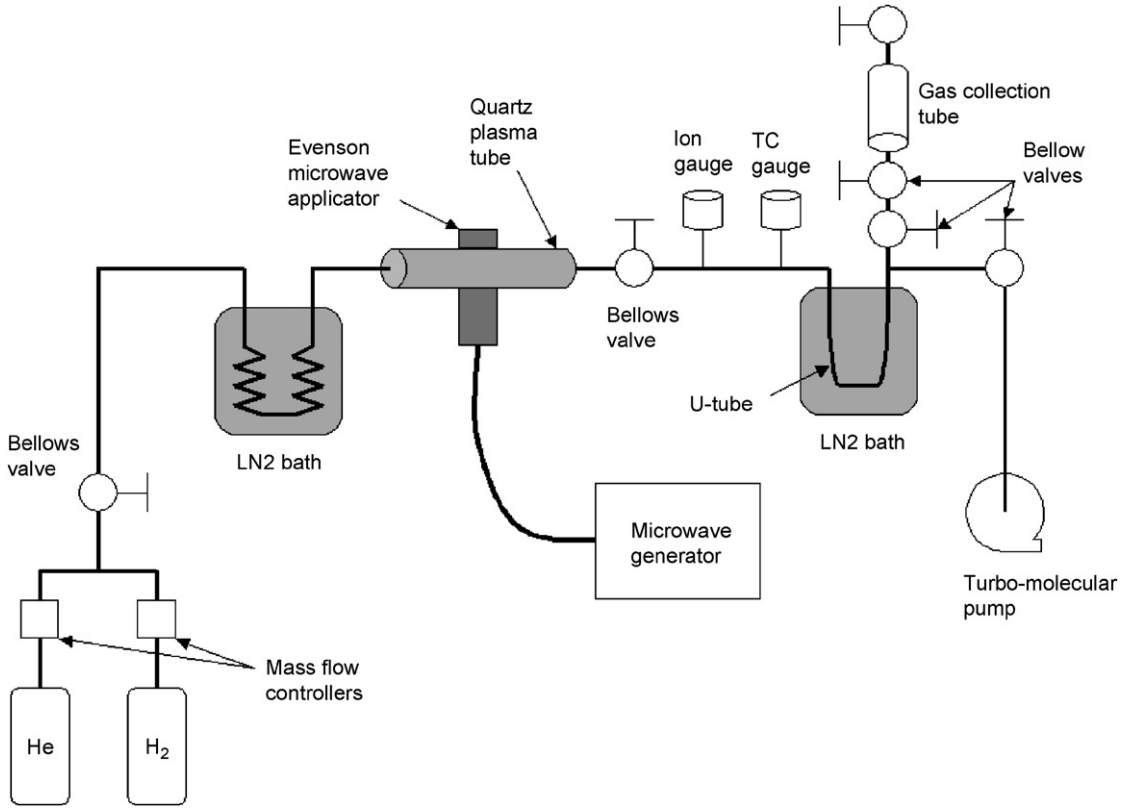

Fig. 1. Microwave plasma system and liquid nitrogen trap system for condensing gases from helium–hydrogen microwave plasmas maintained in an Evenson cavity. The experimental setup comprised a welded-joint stainless steel tubing system (1.27 cm OD × 165 cm length), two mass-flow controllers, two cryotraps, the quartz plasma cell (1.27 cm OD × 31 cm length), ion and TC vacuum gauges (SenTorr, Varian), six bellows valves (welded construction, Nupro U-series, helium leak tested to 4×10^{-9} sccm), and a turbo-molecular pump.

Princeton University, New Jersey using a Nicolet 730 FTIR spectrometer with DTGS detector at resolution of 4 or 0.5 cm^{-1} (high-resolution scan) as described previously [15]. The samples were handled under a inert atmosphere. KH^*I samples were stored under argon for 90 days and analyzed for trapped $H_2(\frac{1}{4})$ molecules before and after storage.

2.5. EUV spectroscopy of electron-bean-excited KH^*Cl

Vibration–rotational emission of $H_2(\frac{1}{4})$ trapped in the lattice of KH^*Cl was investigated by windowless EUV spectroscopy on electron-beam excitation of the crystals using the 12.5 keV electron gun at a beam current of 30–50 μA in the pressure range of $< 10^{-5}$ Torr. Since magnesium is not a catalyst as predicted and experimentally confirmed previously [9–12,21], $MgCl_2$ served as a control. The EUV spectrum was recorded with a photomultiplier tube (PMT). The wavelength resolution was about 2 nm (FWHM) with an entrance and exit slit width of 300 μm. The increment was 0.1 nm and the dwell time was 1 s.

2.6. Liquid-nitrogen collection of $H_2(1/p)$

Condensable gas from helium–hydrogen (90%/10%) microwave plasmas maintained in the Evenson cavity was collected in a high-vacuum (10^{-6} Torr) capable, LN cryotrap shown in Fig. 1. After each plasma run the cryotrap was pumped down to 10^{-5} Torr to remove any non-condensable gases in the system. The pressure was recorded as a function of time as the cryotrap was warmed to room temperature. Typically, about 45 μmoles of condensed gas was collected in a 2 h plasma run. Controls were hydrogen and helium alone.

2.7. Mass spectroscopy

The mass spectra (m/e=1–200) of ultrahigh purity (99.999+ %) hydrogen (Praxair) control samples and samples of the condensable gas from the helium-hydrogen microwave plasmas were recorded with a residual gas analyzer.

2.8. Cryopump collection and mass spectroscopy of $H_2(1/p)$

Gases from a 700 mTorr He/H_2 (90%/10%) Evenson microwave plasma were flowed through a long capillary tube which was maintained in the temperature range ~ 12–17 K by a cryo-cooler. Residual gas was pumped from the capillary, condensable gas was collected over a period of several hours, and the system was evacuated to 10^{-5} Torr to remove any non-condensable gases in the system. Controls were hydrogen and helium alone. Two capillary valves were closed to trap any vaporizing gas as the cryo-cooler was stopped, and the tube

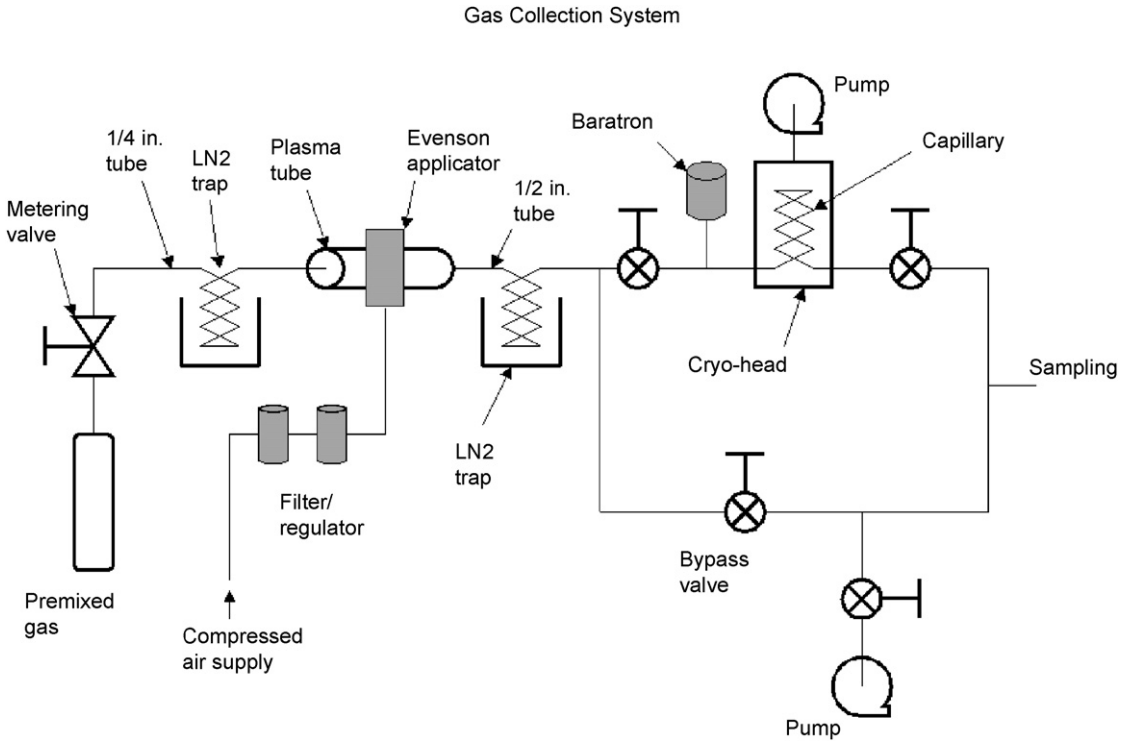

Fig. 2. Microwave plasma system and cryo-cooler trap system maintained at ~ 12–17 K for condensing gases from helium–hydrogen microwave plasmas maintained in an Evenson cavity. The experimental setup comprised a welded-joint stainless steel tubing system, a metering valve, two LN cryotraps, the quartz plasma cell (1.27 cm OD × 31 cm length), a Baratron vacuum gauge, four bellows valves (Nupro B-series, helium leak tested to 4×10^{-9} sccm), a cryo-cooler compressor, a cryohead, a copper capillary tube (0.88 mm ID × 1.7 m length) spiraled on the cold stage of the cryo-head in an evacuated cylindrical chamber, a cryogenic silicon diode temperature sensor, and a turbo-molecular pump.

was warmed to room temperature. Typically about 100 mTorr of gas was collected over a 24 to 48 h period and then analyzed by mass spectroscopy and compared with the results for a control sample collected in the same way, except that no plasma was present.

The system comprised welded stainless steel tubing with metal gasket and rubber o-ring connections as shown in Fig. 2. Premixed He/H_2 (90%/10%) was flowed from a supply bottle through a metering valve and a LN trap just upstream of the plasma tube. A second LN trap downstream of the plasma tube was used to remove any water vapor generated by the plasma. The process gas pressure was monitored by a Baratron absolute pressure gauge upstream of the cryo-head. The cryo-cooler comprised a compressor (CTI Model SC) and cryo-head (CTI Cryogenics Model 22). The principle component of the cryo-head was an evacuated cylindrical chamber of approximately 1 l volume through which the cryogenic refrigerant was circulated in a closed system. A stainless steel cold stage extended from the base of the chamber on the chamber axis. A fabricated cylindrical copper spindle was attached to the existing cold stage by screws. Thermal contact resistance between the spindle and cold stage was minimized by an intervening layer of conducting grease. Approximately 1.7 m of copper capillary tubing, 1.56 mm OD and 0.88 mm ID, was wound onto a spiral groove with 5.5 grooves per cm pitch machined onto the spindle. The capillary tube was fused to the spindle along its span with tin/lead solder. A cryogenic silicon diode temperature sensor was also attached to the spindle just beneath the capillary winding. The sensor output was monitored with a readout (TRI Research Cryo-Controller Model T-2000). The sensor accuracy was better than ±0.1 K in the range 10–300 K.

2.9. Mass spectroscopy

The system was connected to either a Dycor Model DM200MS or Model D200MP mass spectrometer through a sampling tube. A background scan (m/e = 1–200) was acquired for reference before introducing the collected gas to the mass spectrometer. Then, the valve just downstream of the cryo-head was opened, allowing gas to flow into the sample tube and spectrometer. Several scans were taken over a period of about 10 min while gas was slowly drawn out of the capillary tube into the spectrometer.

2.10. NMR of condensed gas

Sealed ^1H NMR samples were prepared by collecting the condensed gas from the cryotrap in $CDCl_3$ solvent (99.99% Cambridge isotopes) in an NMR tube (5 mm OD, 23 cm length, Wilmad) maintained at LN-temperature which was then flame-sealed. Control NMR samples comprised ultrahigh purity

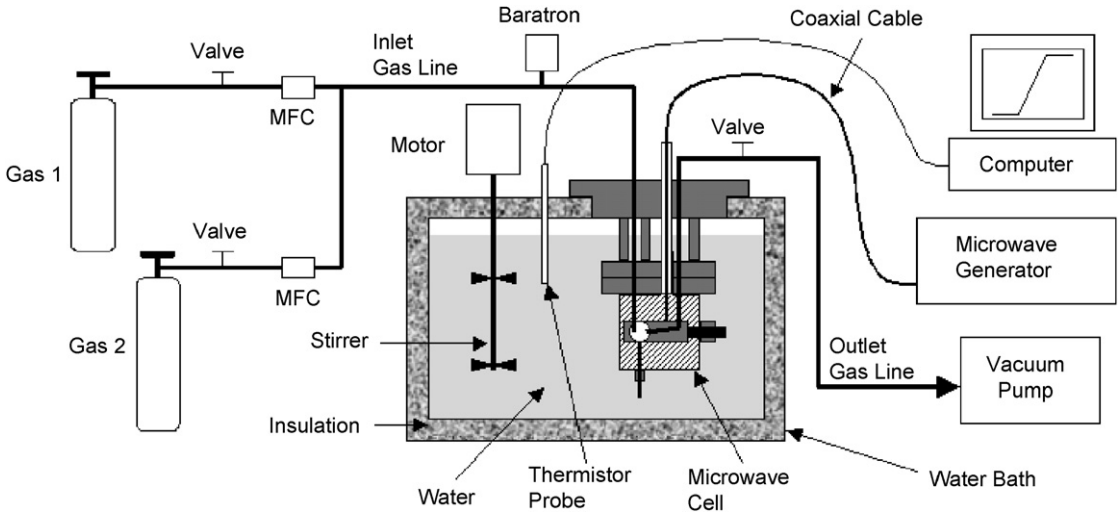

Fig. 3. Schematic of the water bath calorimeter. The Evenson cavity and a plasma-containing section of the quartz tube were fitted with a water-tight stainless steel housing, and the housing and cell assembly were suspended by four support rods from an acrylic plate which held the cell vertically from the top of a water bath calorimeter.

hydrogen (Praxair) and the helium-hydrogen (90%/10%) mixture with $CDCl_3$ solvent. The NMR spectra were recorded with a 300 MHz Bruker NMR spectrometer that was deuterium locked. The chemical shifts were referenced to the frequency of tetramethylsilane (TMS) at 0.00 ppm.

2.11. Gas from decomposition of KH* I

KH*I that was prepared under long duration (two weeks) synthesis according to methods given previously [31,32], and about a 1 g sample was placed in a thermal decomposition reactor under an argon atmosphere. The reactor comprised a $\frac{1}{4}$ in OD by 3 in long quartz tube that was sealed at one end and connected at the open end with Swagelok^{TM} fittings to a T. One end of the T was connected to the NMR tube containing $CDCl_3$ solvent, and the other end was attached to a turbo pump. The apparatus was evacuated to less than 1 milliTorr with the $CDCl_3$ maintained at LN temperature. The sample was heated to 200 °C under vacuum. A valve to the pump was closed, and the sample was heated in the evacuated quartz chamber containing the sample to above 600 °C until the sample melted. Gas released from the sample was collected in the $CDCl_3$ solvent, the NMR tube was sealed and warmed to room temperature, and the NMR spectrum was recorded. Using identical samples, the NMR-tube end of the collection apparatus was connected directly to the sampling port of a quadrupole mass spectrometer to test for hydrocarbon contamination. FTIR was also performed on the released gas for this purpose.

2.12. NMR of gas from decomposition of KH* I

An NMR sample from KH*I provided by BlackLight Power, Inc. was also prepared and analyzed at the Naval Air Warfare Center Weapons Division, Naval Air Warfare Center, China Lake, CA under the same procedure except that the $CDCl_3$ solvent was maintained at ice temperature during hydrogen gas collection, and the NMR spectrum was recorded with a 400 MHz instrument at China Lake. Control NMR samples of ultrapure hydrogen dissolved in $CDCl_3$ solvent were also prepared, and NMR spectra were obtained under conditions matching those of the KH*I-derived samples.

2.13. Water-bath-calorimetry power measurements

The excess power was measured by water bath calorimetry on helium-hydrogen (95%/5%) plasmas maintained in a microwave discharge cell compared to control plasmas with the same input power as described previously [28]. The system is shown in Fig. 3. The water bath was calibrated by a high precision heater and power supply. A high precision linear response thermistor probe (Omega OL-703) recorded the temperature of the 45 L water bath as a function of time for the stirrer alone to establish the baseline. The heat capacity was determined for several input powers, 30, 40, and 50 W ± 0.01 W, and was found to be independent of input power over this power range within ±0.05%. The temperature rise of the reservoir as a function of time gave a slope in °C/s. This slope was baseline corrected for the negligible stirrer power and loss to ambient. The constant known input power (J/s), was divided by this slope to give the heat capacity in J/°C. Then, in general, the total power output from the cell to the reservoir was determined by multiplying the heat capacity by the rate of temperature rise (°C/s) to give J/s.

Since the cell and water bath system were adiabatic, the general form of the power balance equation with the possibility of excess power is

$$P_{in} + P_{ex} - P_{out} = 0, \tag{19}$$

where P_{in} is the microwave input power, P_{ex} is the excess power generated from the hydrogen catalysis reaction, and P_{out} is the thermal power loss from the cell to the water bath. Since the

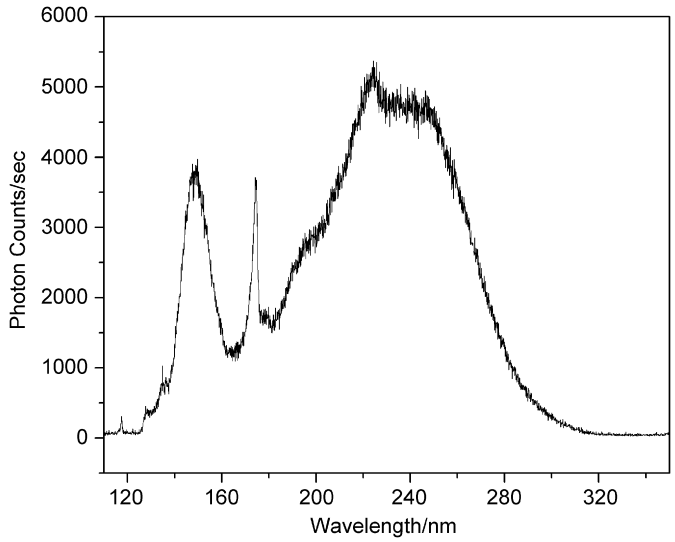

Fig. 4. The 100–350 nm spectrum of a 750 Torr, 12.5 keV-electron-beam-maintained plasma of krypton containing about 1% hydrogen.

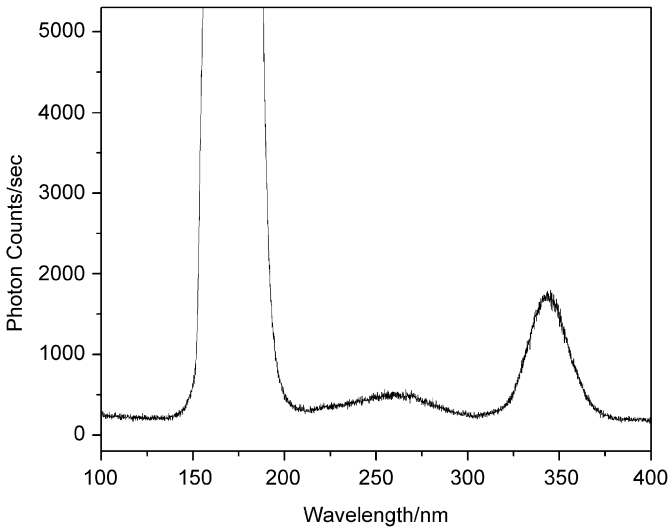

Fig. 5. The 100–350 nm spectrum of a 750 Torr, 12.5 keV-electron-beam-maintained plasma of xenon containing about 1% hydrogen.

cell was surrounded by water that was contained in an insulated reservoir with negligible thermal losses, the temperature response of the thermistor T as a function of time t was determined to be

$$\dot{T}(t) = (1.940 \times 10^5\,\mathrm{J/^\circ C})^{-1} \times P_{\mathrm{out}}, \tag{20}$$

where 1.940×10^5 J/°C is the heat capacity for the least square curve fit of the response to power input for the control experiments ($P_{\mathrm{ex}} = 0$). The slope was recorded for about 2 h after the cell had reached a thermal steady state, to achieve an accuracy of ±1%.

3. Results and discussion

3.1. Identification of $H_2(\frac{1}{4})$ and $H^-(\frac{1}{4})$

3.1.1. Vibration–rotational spectrum of $H_2(\frac{1}{4})$

Molecular formation was anticipated under high-pressure conditions (~ 760 Torr). Thus, EUV spectroscopy of argon-hydrogen plasmas was performed to search for $H_2(\frac{1}{4})$ from $H(\frac{1}{4})$ formed by Ar^+ as a catalyst. The normal incidence spectrometer was used at high pressure which required a window and an electron beam to maintain a plasma. Since the 12.5 keV beam rapidly transfers energy to the target gas and produces a large population of species with energies of a few 10's of eVs of kinetic energy, it was anticipated that the beam could directly or indirectly collisionally excite vibration–rotational states of $H_2(\frac{1}{4})$. The corresponding emission provides a direct measure of the internuclear distance; thus, this method provides the possibility of direct confirmation of $H_2(\frac{1}{4})$.

The continuum excimer bands of krypton and xenon were observed from the emission of 12.5 keV-electron-beam-maintained plasmas of these gases alone or mixed with 1% hydrogen as shown in Figs. 4 and 5, respectively. Rather then just excimer lines, a series of sharp, evenly spaced lines was

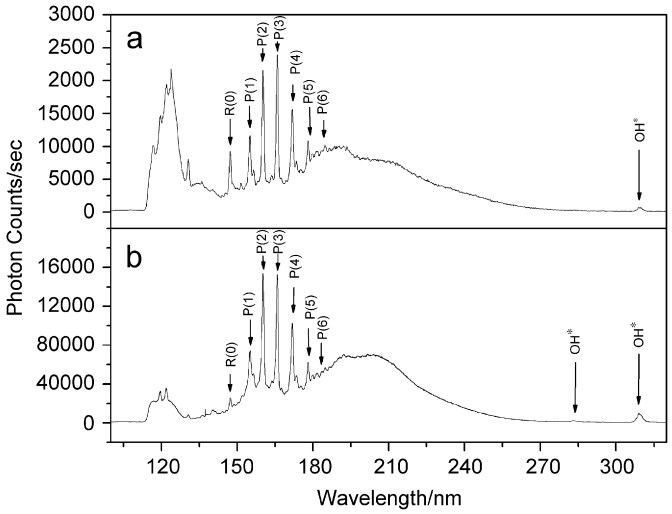

Fig. 6. (a) and (b). The 100–350 nm spectra of 700–800 Torr, 12.5 keV-electron-beam- maintained plasmas of argon containing about 1% hydrogen.

observed in the 150–190 nm region of 700–800 Torr plasmas of argon containing about 1% hydrogen as shown in Figs. 6a and b. The first through third-order spectra are shown in Fig. 7. Lyman α was observed at 121.6 nm with an adjoining H_2 band, the third continuum of Ar was observed at 210 nm [50], and the OH(A − X) bands were observed at 282.7 and 308.6 nm [26,51,52]. The series could not be assigned to any of the controls or known lines of the gases present or any possible contaminant gas.

The only possibilities for sharp peaks of the instrument width are those due to rotation or electronic emission from atoms or ions. The series was not observed when krypton or xenon replaced argon as shown in Figs. 4 and 5, respectively. Additional controls of hydrogen, oxygen, nitrogen, water vapor, and nitrogen–oxygen (50%/50%) were also negative for the series. No hydrogen lines and no strong O I or O II lines matches any

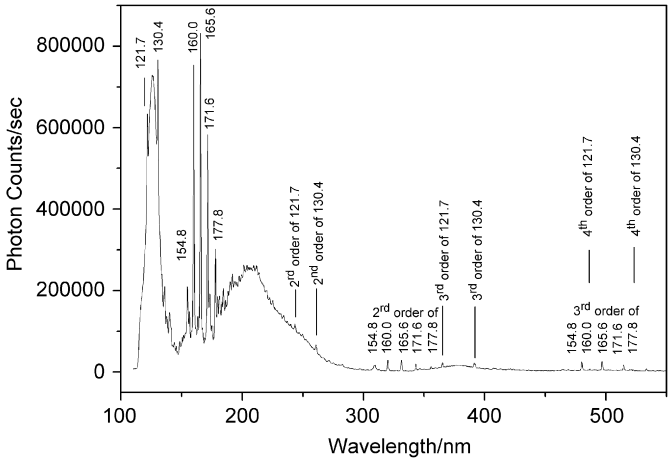

Fig. 7. The 100–560 nm spectrum of 750 Torr, 12.5 keV-electron-beam-maintained plasma of argon containing about 1% hydrogen.

of the lines [53]. In the case that O II is a possibility for some of the lines, other O II lines of equal oscillator strength were not observed. Specifically, the O I line at 130.6 nm having an oscillator strength of over 100 times that of O II lines in this region [53] was weak which made the assignment to O II lines unlikely. No detectable oxygen was observed by the absence of the strong O I line at 130.6 nm [53] in some cases. No combination of O species exclusively matches the evenly spaced lines in this region. The lines were not observed with argon or krypton with oxygen addition up to 50%, and the lines, when observed with argon, 1% hydrogen, and trace oxygen, did not increase in intensity upon addition of additional oxygen. The series was not observed with argon alone, and only Ar VII and Ar VIII are possible in this region which is not possible at this pressure. Furthermore, no argon species match the observed lines [53].

The series identically matched the P branch of $H_2(\frac{1}{4})$ for the vibrational transition $\upsilon=1 \rightarrow \upsilon=0$. P(1), P(2), P(3), P(4), P(5), and P(6) were observed in Fig. 6a at 154.94, 159.74, 165.54, 171.24, 178.14, and 183.14 nm, respectively. The sharp peak at 146.84 nm may be the first member of the R branch, $R(0)$. Other than $R(0)$, R-branch lines appeared to correspond to forbidden transitions in agreement with predictions given in Section 1.2.

The slope of the linear curve-fit of the energies of the peaks shown in Fig. 6a is 0.245 eV with an intercept of 8.224 eV and a sum of residual errors $r^2 < 0.0001$. For the series shown in Fig. 6b, the slope is 0.241 eV with an intercept of 8.21 eV and a sum of residual errors $r^2 < 0.0001$. The energies match those predicted in Eq. (12) very well for $p = 4$. The series matches the predicted $\upsilon = 1 \rightarrow \upsilon = 0$ vibrational energy of $H_2(\frac{1}{4})$ of 8.25 eV (Eq. (9)) and its predicted rotational energy spacing of 0.241 eV (Eq. (10)) with $\Delta J = +1$; $J = 1, 2, 3, 4, 5, 6$ and $\Delta J = -1$; $J = 0$ where J is the rotational quantum number of the final state. Using Eqs. (10) and (11) with the measured rotational energy spacing of 0.24 eV establishes an internuclear distance of $\frac{1}{4}$ that of the ordinary hydrogen species for $H_2(\frac{1}{4})$. This technique which is the best measure of the bond distance of any diatomic molecule identifies and unequivocally confirms $H_2(\frac{1}{4})$.

The Ar^+ catalyst mechanism was confirmed by atmospheric-pressure-plasma-gas flow at 75 sccm and nonflow conditions. Flow does not change known atomic and ionic line emission such as the O I line at 130.6 nm. In contrast, the series assigned to vibration–rotation of $H_2(\frac{1}{4})$ was observed under static conditions; whereas, the series decreased to about 10% with flow indicating a reaction involving the formation of intermediates as predicted.

A possible confirmation of the lines identified in this study has been published previously. Ulrich et al. [50] compared the third continuum of argon gas with a very pure gas and a spectrum in which the gas was slightly contaminated by oxygen as evidenced by the second order of the 130 nm resonance lines at 260 nm. A series of very narrow lines at the instrument width were observed in the 145–185 nm region. These lines shown in Fig. 6 of Ref. [50] matched those in Figs. 6 and 7 having an intensity profile that was characteristic of that of a P-branch. The slope of the linear curve fit is 0.24 eV with an intercept of 8.24 eV which matches Eq. (12) very well for $p = 4$. The series matches the predicted $\upsilon = 1 \rightarrow \upsilon = 0$ vibrational energy of $H_2(\frac{1}{4})$ of 8.25 eV (Eq. (9)) and its predicted rotational energy spacing of 0.24 eV (Eq. (10)) with $\Delta J = +1$; $J = 1, 2, 3, 4, 5, 6$ and $\Delta J = -1$; $J = 0$ where J is the rotational quantum number of the final state. With this assignment, all of the peaks in Fig. 6 of Ref. [50] could be identified; whereas, the evenly spaced lines could not be unambiguously assigned by Ulrich et al. [50]. The series was not observed in krypton and xenon plasmas. The determination of the presence of the common contaminant, hydrogen, in the argon plasmas is warranted in future studies.

3.1.2. NMR and FTIR Identification of $H^-(\frac{1}{4})$

The ^1H MAS NMR spectra relative to external tetramethylsilane (TMS) of KH*Cl samples from independent syntheses and controls were given previously [13,31–33]. The presence of KCl did not shift the resonance of ordinary hydride since the controls comprising an equal molar mixture of KH and KCl and KH as well as KH*Cl showed the same resonance at about 1.3 ppm which was assigned to ordinary hydride ion. KH*Cl samples showed a large distinct upfield resonance at −4.5 ppm which was not observed in either control.

The experimental absolute resonance shift of TMS is −31.5 ppm relative to the proton's gyromagnetic frequency [54,55]. The KH experimental shift of +1.3 ppm relative to TMS corresponding to absolute resonance shift of −30.2 ppm matches very well the predicted shift of $H^-(\frac{1}{1})$ of −30 ppm given by Eq. (17) wherein $p = 0$. The novel peak at −4.5 ppm relative to TMS corresponding to an absolute resonance shift of −36.0 ppm indicates that $p = 4$ in Eq. (17). $H^-(\frac{1}{4})$ is the hydride ion predicted by using K as the catalyst [7,13,21]. Furthermore, the extraordinarily narrow peak-width is indicative of a small hydride ion that is a free rotator.

Samples with the −4.5 ppm peak were analyzed by FTIR spectroscopy to determine if there was any correlation between the −4.5 ppm ^1H NMR peak and possible IR vibration bands, in particular the substitutional H^- U-center band around 502 cm^{-1}. Two KH*Cl samples, 1 and 2, that exhibit equal

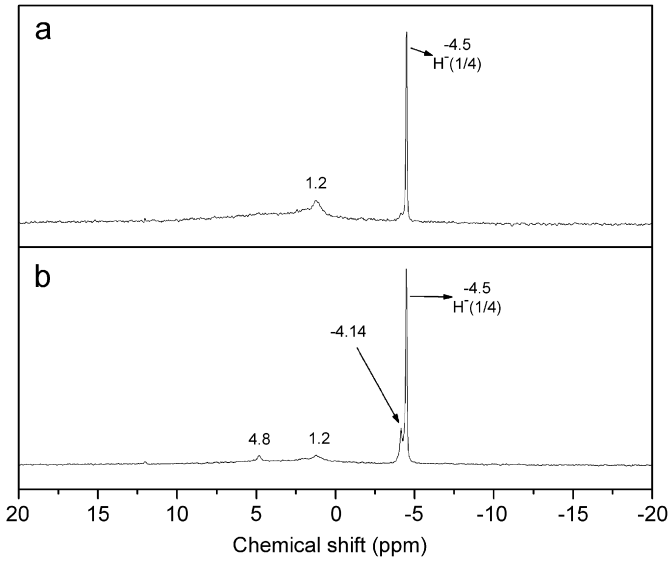

Fig. 8. Solid state ^{1}H NMR spectra of samples 1 and 2. Both samples have a strong −4.5 ppm ^{1}H NMR peak intensity.

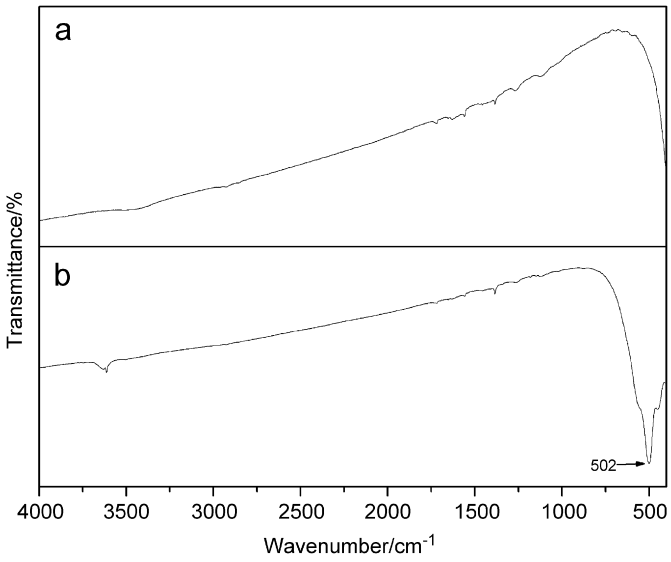

Fig. 9. FTIR spectra of samples 1 and 2 showing that U centered H is not present in sample 1.

intensity peaks at −4.5 ppm in the solid-state ^{1}H NMR spectra (Fig. 8), show markedly different FTIR spectra (Fig. 9), in which sample 2 has the U H^- vibration band at 502 cm^{-1}, while sample 1 does not. Thus, there is no relationship between the presence of U centers and the −4.5 ppm ^{1}H NMR peak. The IR band at 3613 and 3641 cm^{-1} in sample 2 could arise from interstitial H_2O, which corresponds to the 4.8 ppm peak in its ^{1}H NMR spectrum. Since the NMR-FTIR comparison leads to the conclusion that the −4.5 ppm peak in ^{1}H NMR spectrum is not associated with the U H^- vibration band at 502 cm^{-1}, the −4.5 ppm peak in ^{1}H NMR spectrum is assigned to the $H^-(\frac{1}{4})$ ion which matches theoretical predictions and is direct evidence of a lower-energy state hydride ion. The identification

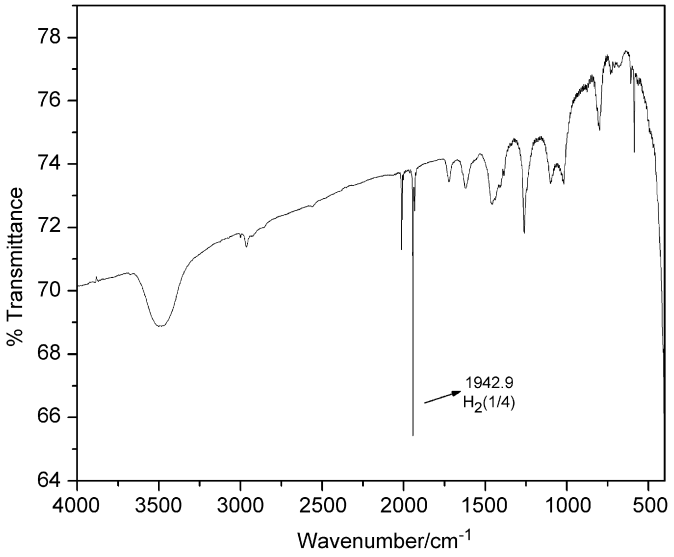

Fig. 10. The high resolution (0.5 cm^{-1}) FTIR spectrum (490–4000 cm^{-1}) of KH*I having a peak assigned to $H^-(\frac{1}{4})$ following storage in an inert atmosphere for 90 days. The 1943 and 2012 cm^{-1} peaks matched the predicted frequencies of ortho- and para-$H_2(\frac{1}{4})$.

of $H^-(\frac{1}{4})$ was confirmed previously by the XPS measurement of its binding energy. The XPS spectrum of KH*I differed from that of KI by having additional features at 8.9 and 10.8 eV that do not correspond to any other primary element peaks but do match the $H^-(n = \frac{1}{4})$ $E_b = 11.2$ eV hydride ion (Eq.(15)) in two different chemical environments.

3.1.3. FTIR identification of $H_2(\frac{1}{4})$

Samples of KH*I having an upfield ^{1}H MAS NMR peak at −4.6 ppm that was assigned to the $H^-(\frac{1}{4})$ ion were stored under argon for 90 days, and the high resolution FTIR spectrum of the solid compound was recorded before and after storage. As shown in Fig. 10, single rotational peaks were observed at 1943 and 2012 cm^{-1} that were unchanged after 90 days of storage. No additional peaks other than those easily assignable to KI were observed. The peak at 1943 cm^{-1} (0.2409 eV) matched the theoretical prediction of 1947 cm^{-1} for $H_2(\frac{1}{4})$. From Eqs. (10)–(11), the unprecedented rotational energy of 4^2 times that of ordinary hydrogen establishes the internuclear distance of $H_2(\frac{1}{4})$ as $\frac{1}{4}$ that of H_2.

As a pair, the 1943 cm^{-1} and 2012 cm^{-1} peaks further match the pattern expected for ortho- and para-$H_2(\frac{1}{4})$ based on the results for H_2. Interstitial H_2 in silicon and GaAs is a nearly free rotator [42–46]. H_2 is FTIR active as well as Raman active due to the induced dipole from interactions with the crystalline site [42]. Furthermore, the Raman and FTIR vibration–rotational bands are split into two components with an intensity ratio of ∼ 3:1 that are assigned to ortho- and para-H_2, respectively. The frequencies differ by 8 cm^{-1} because of the higher rotation-vibrational energy of para relative to ortho-H_2 [42].

The crystalline lattice may also influence the selection rules to permit an otherwise forbidden transition in $H_2(\frac{1}{4})$. The four-significant-figure match for the 1943 cm^{-1} peak and the narrow

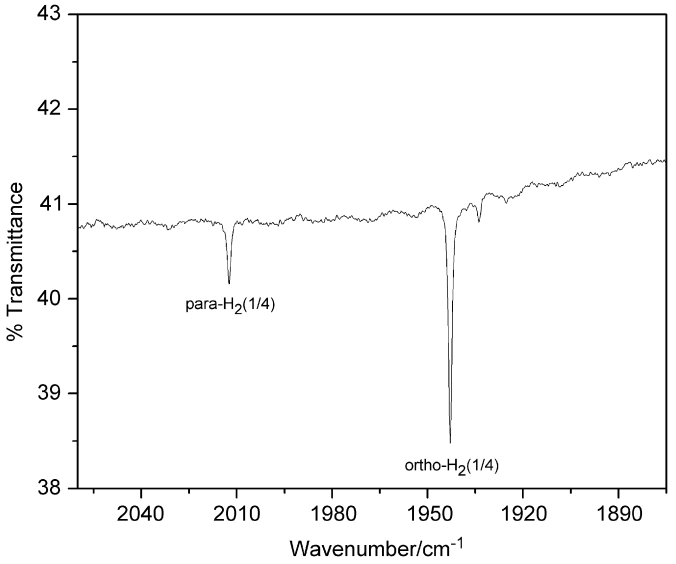

Fig. 11. The high resolution (0.5 cm^{-1}, 160 scans) FTIR spectrum (1875–2060 cm^{-1}) of KH*I showing the 1943/2012 cm^{-1}-peak-intensity ratio of 3:1 which is characteristic of ortho–para hydrogen splitting. The observed ortho–para splitting of 69 cm^{-1} matched that predicted.

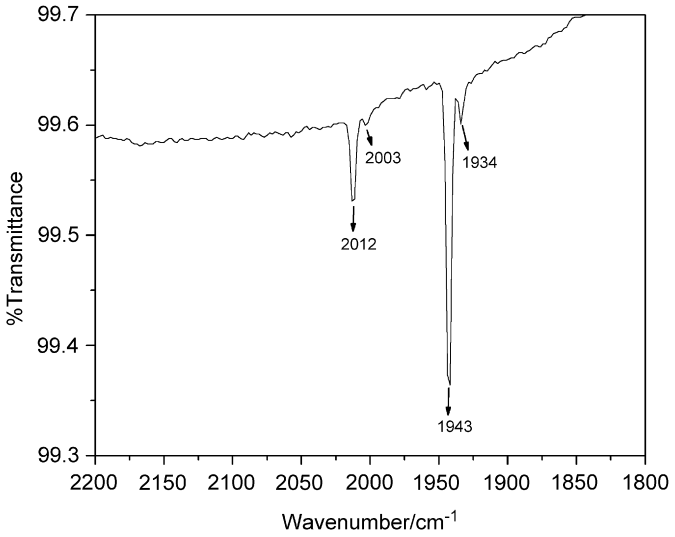

Fig. 12. The repeat FTIR spectrum (490–4000 cm^{-1}) of Fig. 11 with 1028 scans at a resolution of 4 cm^{-1}. Two sets of ortho–para peaks of the same 3:1 intensity ratio and splitting were resolved. The shift may be due to the presence of two phases in KH*I—one due to $H_2(\frac{1}{4})$ in KH*I and one due to $H_2(\frac{1}{4})$ in KI.

peak width that was observed to be as low as 1 cm^{-1} in some samples indicates that $H_2(\frac{1}{4})$ can rotate freely inside of the crystal and confirms its small size corresponding to $\frac{1}{4}$ the dimensions of ordinary hydrogen. Furthermore as shown in Fig. 11, the intensity ratio of the 1943 and 2012 cm^{-1} peaks is about 3:1 which matches the hydrogen ortho–para ratio at noncryogenic temperatures. In this case, the proposed para-$H_2(\frac{1}{4})$ rotational frequency is 69 cm^{-1} higher than that of ortho-$H_2(\frac{1}{4})$.

The splitting can easily be calculated from the result of Lavrov and Weber [43] for free H_2 using the Morse-potential expansion with an inter nuclear distance of $\frac{1}{4}$ that of H_2:

$$\frac{\Delta_{H_2(1/4)}}{\Delta_{H_2}} = \frac{\frac{12(256)B_e^2}{\hbar 16\omega_e}\left(\frac{4\hbar}{\mu 256\omega_e^2}\sqrt{\frac{2}{\mu 16 B_e}} - 1\right)}{\frac{12B_e^2}{\hbar\omega_e}\left(\frac{a\hbar}{\mu\omega_e^2}\sqrt{\frac{2}{\mu B_e}} - 1\right)}. \quad (21)$$

In the case that $1 \ll (a\hbar/\mu\omega_e^2)\sqrt{2/\mu B_e}$

$$\Delta_{H_2(1/4)} = 16\Delta_{H_2} = 4^2\Delta_{H_2} = 70.4\,cm^{-1}, \quad (22)$$

where the calculated H_2 result of 4.4 cm^{-1} [43] allowed for the cancellation of the curve-fit parameter a. The result agrees well with the observed ortho–para splitting of 69 cm^{-1}. Given the frequency match of the 1943 peak, the 3:1 intensity ratio, the match of the frequency difference between the peaks, and the absence of any known alternative wherein hydrogen is the only known species that exhibits single ro-vibrational transitions in a solid matrix, the 1943 and 2012 cm^{-1} peaks are assigned to the $J = 0$–1 rotational transitions of ortho- and para-$H_2(\frac{1}{4})$, respectively.

Two sets of ortho–para peaks of the same 3:1 intensity ratio and splitting were resolved with the accumulation of 1028 scans as shown in Fig. 12. The shift may be due to the presence of two phases in KH*I—one due to $H_2(\frac{1}{4})$ in KH*I and one due to $H_2(\frac{1}{4})$ in KI as discussed for the case of KH*Cl in Section 3.1.4.

3.1.4. $H_2(\frac{1}{4})$ rotational spectrum by EUV spectroscopy of electron-beam-excited KH*Cl

Since the rotational emission of $H_2(\frac{1}{4})$ was observed in crystals of KH*I having a peak assigned to $H^-(\frac{1}{4})$ (Section 3.1.3) and the vibration–rotational emission of $H_2(\frac{1}{4})$ was observed from 12.5 keV-electron-beam-maintained plasmas of argon with 1% hydrogen due to collisional excitation of $H_2(\frac{1}{4})$ (Section 3.1.1), $H_2(\frac{1}{4})$ trapped in the lattice of KH*Cl was investigated by windowless EUV spectroscopy on electron-beam excitation of the crystals using the 12.5 keV electron gun at a beam current of 30–50 μA in the pressure range of $< 10^{-5}$ Torr. No emission was observed from crystals of $MgCl_2$ over the range 5–560 nm except for a weak continuum band in the 200–300 nm region as shown in Fig. 13. The electron-beam-excited KH*Cl crystal having a −4.4 ppm NMR peak assigned to $H^-(\frac{1}{4})$ is shown in Fig. 14. No emission was observed outside of the 150–350 nm region other than Lyman α at 121.6 nm. A broad continuum was observed in the 160–180 nm region, the same region as the series assigned to the P branch of $H_2(\frac{1}{4})$ as given in Section 3.1.1. An additional series of evenly spaced lines was observed in the 220–310 nm region. The beam was focused to another spot, and Lyman α was also observed at 121.6 nm. At the second position, the series of lines in the220–310 nm region were well resolved as shown in Fig. 15.

The series matched the spacing and intensity profile of the P branch of $H_2(\frac{1}{4})$ given in Section 3.1.1. P(1), P(2), P(3),

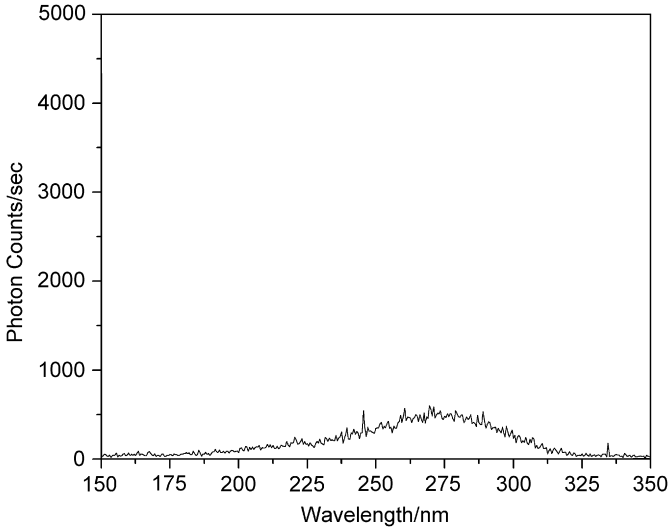

Fig. 13. The 150–350 nm spectrum of electron-beam-excited $MgCl_2$.

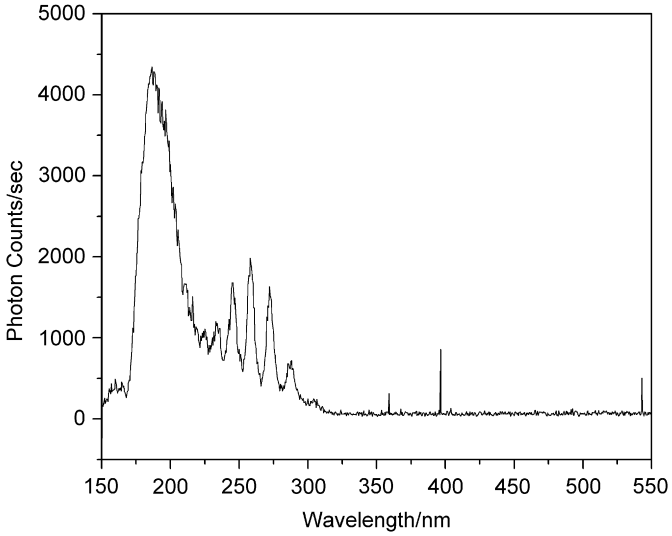

Fig. 14. The 150–550 nm spectrum of electron-beam-excited KH*Cl having a −4.4 ppm NMR peak assigned to $H^-(\frac{1}{4})$.

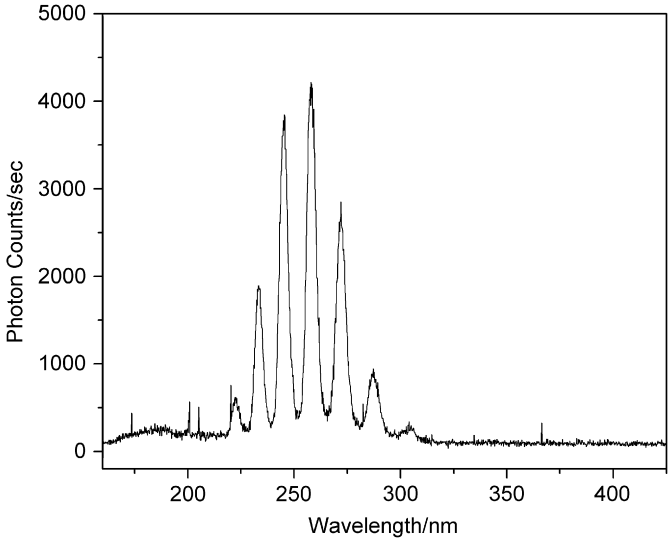

Fig. 15. The 150–450 nm spectrum of electron-beam-excited KH*Cl having a −4.4 ppm NMR peak assigned to $H^-(\frac{1}{4})$ at a second spot on the crystal.

P(4), P(5), P(6), and P(7) were observed at 222.4, 233.5, 245.2, 258.2, 272.1, 278.0, and 304.0 nm, respectively. The slope of the linear curve-fit of the energies of the peaks shown in Fig. 15 is 0.245 eV with an intercept of 5.81 eV and a sum of residual errors $r^2 < 0.0001$. The slope matches the predicted rotational energy spacing of 0.241 eV (Eq. (10); $p = 4$) with $\Delta J = +1$; $J = 1, 2, 3, 4, 5, 6, 7$ where J is the rotational quantum number of the final state. $H_2(\frac{1}{4})$ is a free rotator, but is not a free vibrator which is similar to the case of interstitial hydrogen in silicon discussed in Section 3.1.3. The observed intercept of 5.81 eV is shifted from the predicted $\upsilon = 1 \rightarrow \upsilon = 0$ vibrational energy of $H_2(\frac{1}{4})$ of 8.25 eV (Eq. (9)) by about twice the percentage as that of interstitial H_2 in silicon [42–46]. In the latter case, vibrational energy of free H_2 is 4161 cm^{-1}, whereas the vibrational peaks in silicon are observed at 3618 and 3627 cm^{-1} corresponding to ortho- and para-H_2, respectively [42]. In the former case the shift is about 30% lower possibly due to an increase in the effective mass from coupling of the molecular vibrational mode with the crystal lattice. Furthermore, the observation of a continuum band in the region of the predicted $\upsilon = 1 \rightarrow \upsilon = 0$ vibrational energy of $H_2(\frac{1}{4})$ and a shifted band having a free-rotator state of $H_2(\frac{1}{4})$ may be due to the presence of two phases in KH*Cl—one due to $H_2(\frac{1}{4})$ in KH*Cl and one due to $H_2(\frac{1}{4})$ in KCl.

Using Eqs. (10) and (11) with the measured rotational energy spacing of 0.24 eV establishes an internuclear distance of $\frac{1}{4}$ that of the ordinary H_2 for $H_2(\frac{1}{4})$. This technique which is the best measure of the bond distance of any diatomic molecule identifies and unequivocally confirms $H_2(\frac{1}{4})$ as also given by the electron-beam plasma spectroscopy and the FTIR spectra given in Sections 3.1.1 and 3.1.3, respectively.

3.2. Isolation and characterization of $H_2(1/p)$

3.2.1. Cryotrap pressure

Helium–hydrogen (90%/10%) gas was flowed through the microwave tube and the cryosystem for 2 h with the trap cooled to LN temperature. No change in pressure over time was observed when the dewar was removed, and the system was warmed to room temperature as shown in Fig. 16. The experiment was repeated under the same conditions but with a plasma maintained with 60 W forward microwave power and 10 W reflected. In contrast to the control case, a liquid-nitrogen-condensable gas was generated in the helium–hydrogen plasma reaction since the pressure due to the reaction product rose from 10^{-5} to 3 Torr as the cryotrap warmed to room temperature.

3.2.2. Mass spectroscopy

The mass spectrum for the gases collected in the cryotrap from the He/H_2 (90%/10%) plasma over the range $m/e = 1$–200

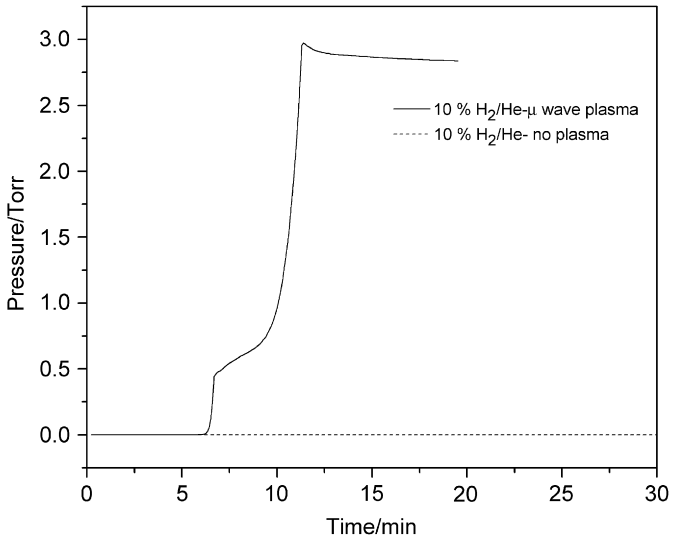

Fig. 16. The pressure as a function of time after the liquid nitrogen dewar was removed from the U-tube cryotrap following 2 h of helium–hydrogen (90%/10%) gas flow through the microwave tube and the cryosystem shown in Fig. 1 without plasma (dotted) and with a plasma maintained with 60 W forward microwave power and 10 W reflected (solid). A liquid-nitrogen condensable gas product was only observed for the plasma reaction run.

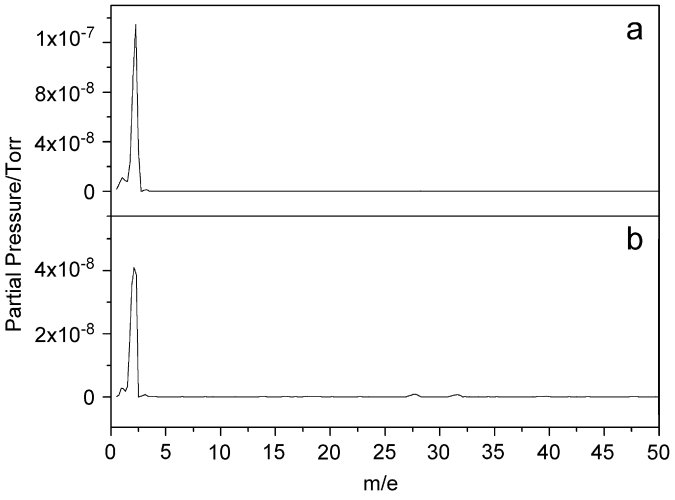

Fig. 17. The mass spectra ($m/e = 1$–50) for the gases collected from He/H_2 (90%/10%) microwave plasmas (IP = 70 eV). (a) The mass spectrum of the gas condensed by the LN cryotrap over 2 h. Only hydrogen peaks were observed which identified the liquid-nitrogen-condensable gas as hydrogen. (b) The mass spectrum of plasma gas collected by the cryo-cooler. The $m/e = 2$ peak was 40–50 times more intense than the $m/e = 28$ and 32 peaks that were assigned to very trace residual air contamination. When corrected for ionization efficiency, H_2 ($m/e = 2$) was determined to be ~ 500 times more abundant than the background.

showed that the LN-condensable gas was highly pure hydrogen. The mass spectrum for the ($m/e = 1$–50) region is shown in Fig. 17a. The mass spectrum ($m/e = 1$–200) for the gases collected in the cryo-cooler from the He/H_2 (90%/10%) plasma only showed peaks in the ($m/e = 1$–50) region. The $m/e = 2$ peak shown in Fig. 17b was 40–50 times more intense than the $m/e = 28$ (nitrogen), $m/e = 32$ (oxygen), and $m/e = 40$ (argon)

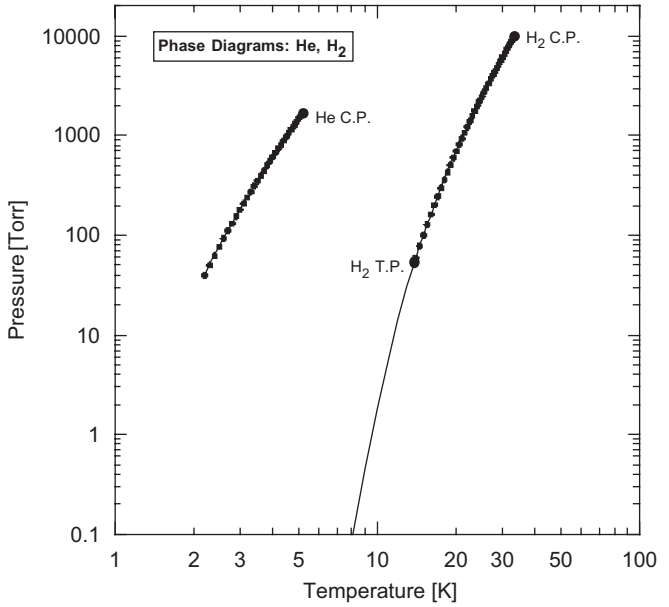

Fig. 18. The phase diagram of hydrogen and helium. Since it is not possible to condense ordinary hydrogen below ~ 50 Torr at 12–17 K, the $m/e = 2$ peak of the mass spectrum (Fig. 17) of plasma gas collected by the cryo-cooler at 700 mTorr that was not removed at 10^{-5} Torr indicates that a novel hydrogen gas formed in the plasma reaction between hydrogen and helium.

peaks that were assigned to very trace residual air contamination. Whereas, without the plasma, the mass $m/e = 2$ peak was present in only trace concentration (~ 10^{-10} Torr) compared with the air contaminant gases that were also present in low abundance (~ 10^{-9} Torr). Von Engel [56] gives the efficiency of production of various common ions at 70 eV and shows that the cross section for the formation of H_2^+ is 10% of that of air contaminants at the same partial pressure. Thus, hydrogen was ~ 500 times more abundant in the collected gas than air contaminants which may have originated through back-streaming in the mass spectrometer.

The phase diagram of helium and hydrogen is shown in Fig. 18 that was plotted from data given by Lide [57] and extended to lower pressures and temperatures using the Clausius–Clapeyron equation [58]. It is not possible to condense ordinary hydrogen below ~ 50 Torr at 12–17 K as shown by its phase diagram. The condensation of a $m/e = 2$ gas in the temperature range of 12–17 K at 700 mTorr that was not removed at 10^{-5} Torr indicates that a novel hydrogen gas formed in the plasma reaction between hydrogen and helium. The results are even more dramatic in the case of the condensation of a $m/e = 2$ gas in the temperature range of 77 K using the LN cryotrap.

3.2.3. ^1H NMR

The ^1H NMR on $CDCl_3$ showed only a singlet solvent ($CHCl_3$) peak at 7.26 ppm relative to tetramethylsilane (TMS) with small ^{13}C side bands. The ^1H NMR on ultrahigh purity hydrogen dissolved in $CDCl_3$ relative to tetramethylsilane (TMS) showed only singlet peaks at 7.26, 4.63, and 1.57 ppm corresponding to $CHCl_3$, H_2, and H_2O, respectively. The chemical shifts of the $CHCl_3$ and H_2O peaks

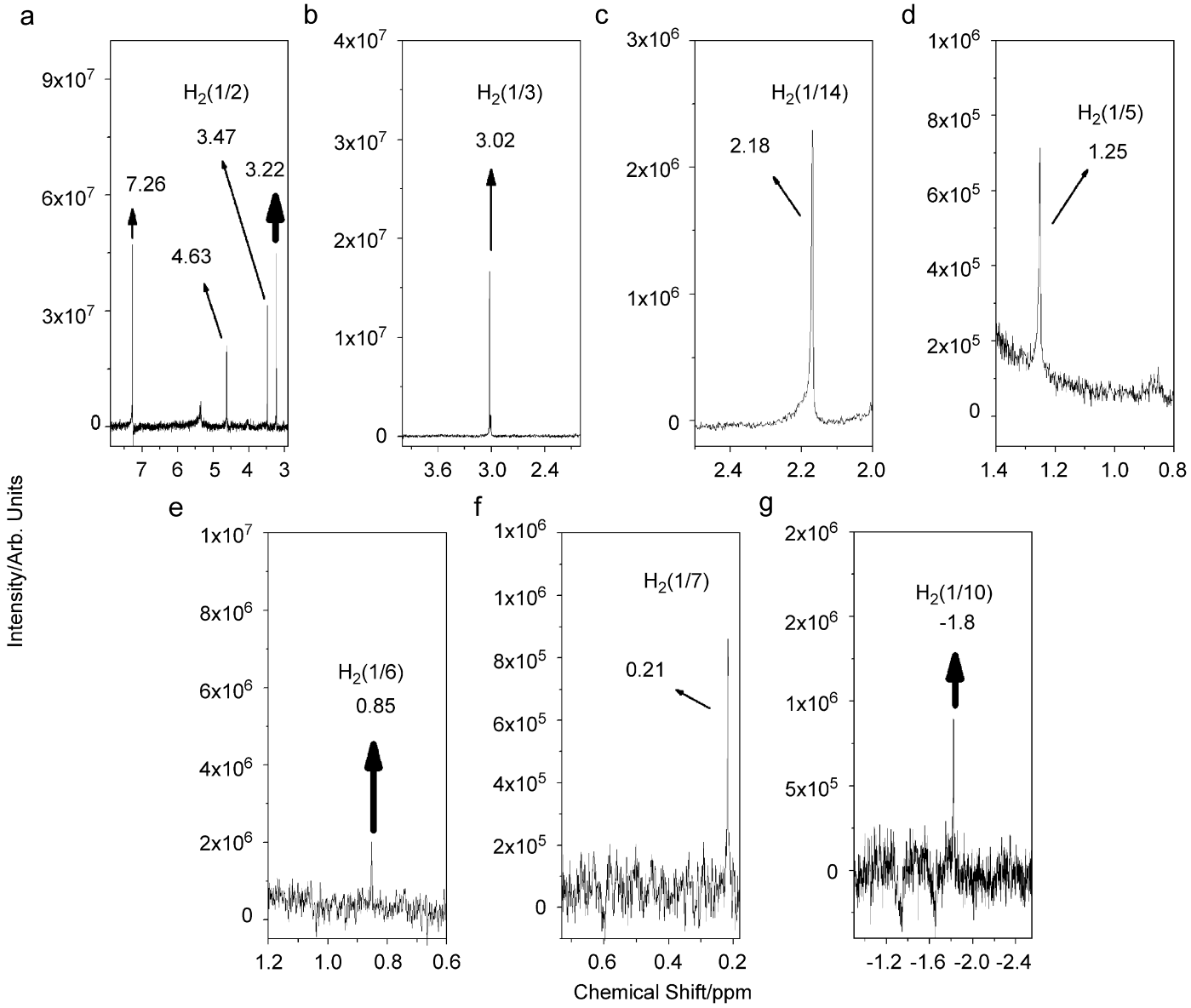

Fig. 19. (a)–(g). ^{1}H NMR spectra on sealed samples of liquid-nitrogen-condensable helium–hydrogen plasma gases dissolved in $CDCl_3$ relative to tetramethylsilane (TMS). The solvent peak was observed at 7.26 ppm, the H_2 peak was observed at 4.63 ppm, and a singlet at 3.22 ppm matched silane. Singlet peaks upfield of H_2 were observed at 3.47, 3.02, 2.18, 1.25, 0.85, 0.21, and −1.8 ppm relative to TMS corresponding to solvent-corrected absolute resonance shifts of −29.16, −29.61, −30.45, −31.38, −31.78, −32.42, and −34.43 ppm, respectively. Using Eq. (14), the data indicates that $p = 2, 3, 4, 5, 6, 7$, and 10, respectively. The data matched the series $H_2(\frac{1}{2})$, $H_2(\frac{1}{3})$, $H_2(\frac{1}{4})$, $H_2(\frac{1}{5})$, $H_2(\frac{1}{6})$, $H_2(\frac{1}{7})$, and $H_2(\frac{1}{10})$.

matched the literature values of 1.56 and 7.26 ppm, respectively [59]. The error in the observed peaks was determined to be ±0.01 ppm. The ^{1}H NMR spectroscopic results of the control prepared from the reagent helium–hydrogen mixture was the same as that of the high purity hydrogen control.

H_2 has been characterized by gas phase ^{1}H NMR. The experimental absolute resonance shift of gas-phase TMS relative to the proton's gyromagnetic frequency is −28.5 ppm [60]. H_2 was observed at 0.48 ppm compared to gas phase TMS set at 0.00 ppm [61]. Thus, the corresponding absolute H_2 gas-phase resonance shift of −28.0 ppm (−28.5 + 0.48) ppm was in excellent agreement with the predicted absolute gas-phase shift of −28.01 ppm given by Eq. (14).

The absolute H_2 gas-phase shift can be used to determine the solvent shift for H_2 dissolved in $CDCl_3$. The correction for the solvent shift can then be applied to other peaks to determine the gas-phase absolute shifts to compare to Eq. (14). The shifts of all of the peaks were relative to liquid-phase TMS which has an experimental absolute resonance shift of −31.5 ppm relative to the proton's gyromagnetic frequency [54,55]. Thus, the experimental shift of H_2 in $CDCl_3$ of 4.63 ppm relative to liquid-phase TMS corresponds to an absolute resonance shift of −26.87 ppm (−31.5 + 4.63 ppm). Using the absolute

H_2 gas-phase resonance shift of −28.0 ppm corresponding to 3.5 ppm (−28.0–(−31.5 ppm)) relative to liquid TMS, the $CDCl_3$ solvent effect is 1.13 ppm (4.63–3.5 ppm) which is comparable to that of hydrocarbons [59].

^{1}H NMR spectra on sealed samples of condensable helium–hydrogen plasma gases dissolved in $CDCl_3$ relative to tetramethylsilane (TMS) are shown in Figs. 19(a)–(f). The solvent peak was observed at 7.26 ppm, the H_2 peak was observed at 4.63 ppm, and a singlet at 3.22 ppm matched silane. Small ^{29}Si side bands were observed for the latter. The source was determined to be hydrogen-plasma reduction of the quartz tube. The peak was unchanged after three weeks at room temperature. No other silanes, silane decomposition species, or solvent decomposition species were observed even after one month of repeat NMR analysis. Since the plasma gases were first passed through an LN trap before the plasma cell, and the cryotrap was high-vacuum (10^{-6} Torr) capable, no hydrocarbons were anticipated. This was confirmed by mass spectroscopic and FTIR analysis that showed only water vapor in addition to silane as contaminants. Again, the source was determined to be hydrogen-plasma reduction of the quartz tube.

As further shown in Figs. 19(a)–(g), singlet peaks upfield of H_2 were observed at 3.47, 3.02, 2.18, 1.25, 0.85, 0.21, and −1.8 ppm relative to TMS corresponding to solvent-corrected absolute resonance shifts of −29.16, −29.61, −30.45, −31.38, −31.78, −32.42, and −34.43 ppm, respectively. Using Eq. (14), the data indicates that $p = 2, 3, 4, 5, 6, 7$, and 10, respectively. The data matched the series $H_2(\frac{1}{2})$, $H_2(\frac{1}{3})$, $H_2(\frac{1}{4})$, $H_2(\frac{1}{5})$, $H_2(\frac{1}{6})$, $H_2(\frac{1}{7})$, and $H_2(\frac{1}{10})$.

The observed series has implications for the catalysis reactions and the corresponding rates. The second ionization energy of helium is 54.4 eV; thus, the ionization reaction of He^+ to He^{2+} has a net enthalpy of reaction of 54.4 eV which is equivalent to $2 \cdot 27.2$ eV. Since the products of the catalysis reaction have binding energies of $m \cdot 27.2$ eV, they may further serve as catalysts by the so-called exothermic disproportionation reactions where one atom goes to a lower state while another goes to a higher state [2,3]. EUV spectroscopy was recorded on microwave discharges of helium with 2% hydrogen. Novel emission lines were observed with energies of $q \cdot 13.6$ eV, $q = 1, 2, 3, 7, 9, 11$ or $q \cdot 13.6$ eV, $q = 4, 6, 8$ less 21.2 eV corresponding to inelastic scattering of these photons by helium atoms due to excitation of He $(1s^2)$ to He $(1s^1 2p^1)$. Alternatively, the photon emission of the intermediate formed by resonant nonradiative energy transfer to the catalyst He^+ is partially quenched by the strong He $(1s^2)$ to He $(1s^1 2p^1)$ transition [49,50]. As given previously [49,50], the quenching reaction is selection rule dependent and results in the emission of a photon less energetic by 21.2 eV. Thus, helium ion catalyzes $H[a_H]$ to $H[\frac{a_H}{3}]$ as shown in Eqs. (5)–(7) of Ref. [3]. Further disproportionation reactions may then proceed:

$$H\left[\frac{a_H}{3}\right] + H\left[\frac{a_H}{3}\right] \rightarrow H\left[\frac{a_H}{4}\right] + H\left[\frac{a_H}{2}\right] + 27.2\,\text{eV}. \qquad (23)$$

The observed, strong 45.6 nm emission [1–3] indicates that the reaction rate for Eq. (23) is very high. Thus, species corresponding to the product atoms such as $H(\frac{1}{2})$ and $H(\frac{1}{4})$ with

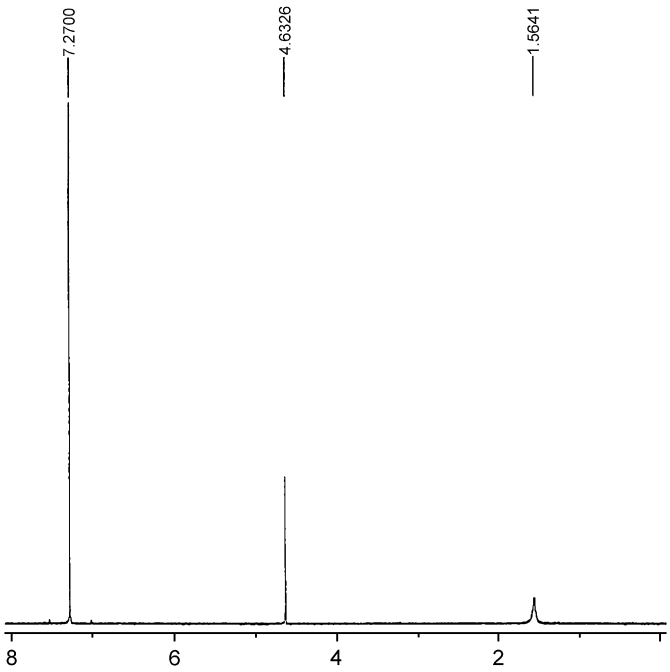

Fig. 20. The ^{1}H NMR spectrum recorded at China Lake on a sealed sample of ultrahigh purity hydrogen dissolved in $CDCl_3$ relative to external tetramethylsilane (TMS). Singlet peaks were observed at 7.27, 4.63, and 1.56 ppm corresponding to $CHCl_3$, H_2, and H_2O, respectively.

products from further transitions having $p > 4$ as given in Refs. [2,3] are anticipated as the reaction products.

The results of the ^{1}H NMR spectra recorded at China Lake on ultrahigh purity hydrogen and gases from the thermal decomposition of KH*I dissolved in $CDCl_3$ relative to TMS are shown in Figs. 20 and 21, respectively. Results matching those shown in Figs. 20 and 21 were obtained at BlackLight Power, Inc. In addition, these samples were determined not to contain hydrocarbons by mass spectroscopy and FTIR analysis. H_2 and H_2O were observed at 4.63 and 1.42 ppm, respectively. The water shift may be attributed to a temperature effect. Singlet peaks upfield of H_2 were observed from the KH*I-derived sample at 3.02, 2.18, 0.85, and 0.22 ppm relative to TMS corresponding to solvent-corrected absolute resonance shifts of −29.61, −30.45, −31.78, and −32.41 ppm, respectively. Using Eq. (14), the data indicates that $p = 3$, 4, 6, and 7, respectively. The data matched the series $H_2(\frac{1}{3})$, $H_2(\frac{1}{4})$, $H_2(\frac{1}{6})$, and $H_2(\frac{1}{7})$. The observed products were consistent with those anticipated with the catalysis of H by K to form $H(\frac{1}{4})$ and subsequent disproportionation reactions [2,3,13,21,22,33].

As shown in Figs. 19 and 21, the observation of the series of singlet peaks upfield of H_2 with a predicted integer spacing of 0.64 ppm at 3.47, 3.02, 2.18, 1.25, 0.85, and 0.22 ppm identified as the consecutive series $H_2(\frac{1}{2})$, $H_2(\frac{1}{3})$, $H_2(\frac{1}{4})$, $H_2(\frac{1}{5})$, $H_2(\frac{1}{6})$, and $H_2(\frac{1}{7})$ and $H_2(\frac{1}{10})$ at −1.8 ppm provides powerful confirmation of the existence of $H_2(1/p)$. Furthermore, the ^{1}H NMR spectra of gases from the thermal decomposition of KH*I matched those of LN-condensable hydrogen. This provides strong support that compounds such as KH*I contain hydride ions $H^-(1/p)$ in the same fractional quantum state p

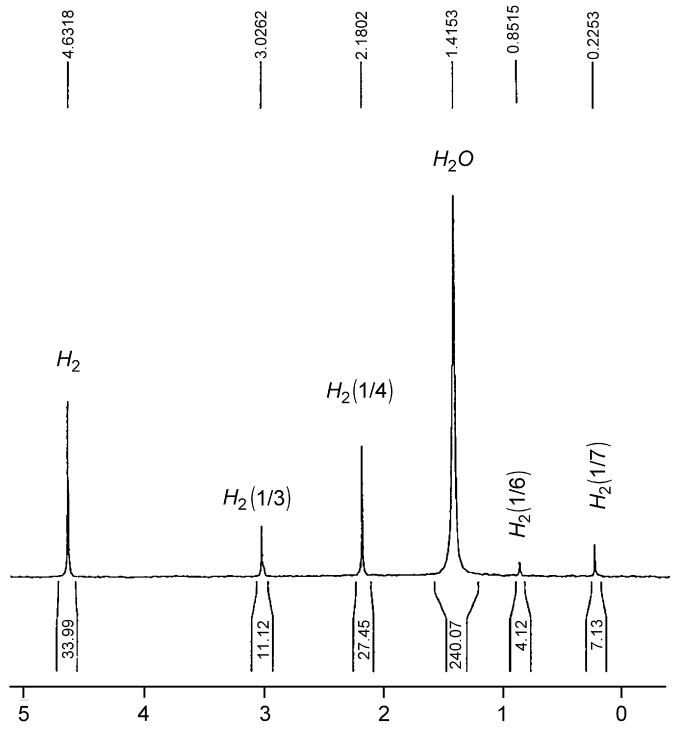

Fig. 21. The ^{1}H NMR spectrum recorded at China Lake on gases from the thermal decomposition of KH*I dissolved in $CDCl_3$ relative to tetramethylsilane (TMS). H_2 and H_2O were observed at 4.63 and 1.42 ppm, respectively. Singlet peaks upfield of H_2 were observed at 3.02, 2.18, 0.85, and 0.22 ppm relative to TMS corresponding to solvent-corrected absolute resonance shifts of −29.61, −30.45, −31.78, and −32.41 ppm, respectively. Using Eq. (14), the data indicates that $p = 3, 4, 6$, and 7, respectively. The data matched the series $H_2(\frac{1}{3})$, $H_2(\frac{1}{4})$, $H_2(\frac{1}{6})$, and $H_2(\frac{1}{7})$.

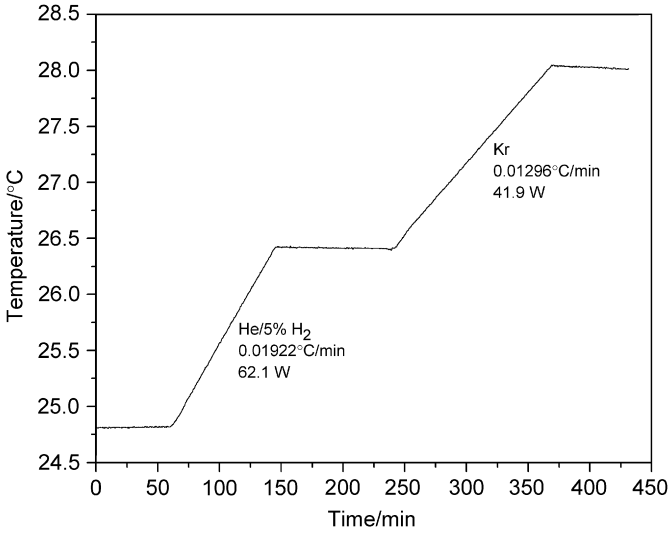

Fig. 22. The $T(t)$ water bath response to stirring and then with selected panel meter readings of the constant forward and reflected microwave input power to helium–hydrogen (95%/5%) mixture was recorded. Krypton control was run at identical microwave input power readings, and the microwave input power was determined to be 41.9 ± 1 W. From the difference in the $T(t)$ water bath response, the excess power of the helium–hydrogen plasma reaction was determined to be 20.2 ± 1 W.

as the corresponding observed $H_2(1/p)$. Observational agreement with predicted positions of upfield-shifted ^{1}H MAS NMR peaks (Eq. (17)) of the compounds [13,31–33], catalyst reactions [13,21,22,24,25], and spectroscopic data [21] supports this conclusion. On this basis, possibilities for advanced technologies are discussed in Section 3.2.5.

3.2.4. Power balance of the helium–hydrogen microwave plasma

The water bath calorimeter is an absolute standard and indicated $P_{in} = 41.9 \pm 1$ W input power at the selected diode settings for all control plasmas. From these results, power input to the helium–hydrogen plasma was confidently known as the diode readings were identically matched for the controls. For example, the $T(t)$ water bath response to stirring and then with selected panel meter readings of the constant forward and reflected microwave input power to krypton was recorded as shown in Fig. 22. Using the corresponding $\dot{T}(t)$ in Eq. (20), the microwave input power was determined to be 41.9 ± 1 W. The $T(t)$ response was significantly increased for helium–hydrogen (95%/5%) as shown in Fig. 22. From the difference in the $T(t)$ water bath response, the output and excess power of the helium–hydrogen plasma reaction was determined to be 62.1 ± 1 W and 20.2 ± 1 W using Eqs. (20) and (19) with the measured $P_{in} = 41.9 \pm 1$ W. The sources of error were the error in the calibration curve (±0.05 W) and the measured microwave input power (±1 W). The propagated error of the calibration and power measurements was ±1 W. Given an excess power of 20.2 W in 3 cm^3 and a helium–hydrogen (95%/5%) flow rate of 10 sccm, the excess power density and energy balance were high, 6.7 W/cm^3 and -5.4×10^4 kJ/mole H_2 (280 eV/H atom), respectively. These results have been confirmed [27].

In addition to high energy spectral emission as shown in Sections 3.1.1, 3.1.4, previously [1–3], other indications of very energetic reactions are observed. For example, population inversion has been observed from microwave plasmas which contain atomic hydrogen with the presence of a catalyst [24–26] as well as novel spectral lines [1–3], and selective, extraordinary H broadening without a conventional explanation such as applied-field acceleration [17,18]. The observation of the $H_2(\frac{1}{4})$ rotational lines reported in Section 3.1.1 from Ar/H_2 plasmas but not from Kr/H_2 and Xe/H_2 plasmas also matches predictions. $H_2(\frac{1}{4})$ was confirmed in Section 3.1.3 by the observation of 1943 and 2012 cm^{-1} peaks in the high-resolution (0.5 cm^{-1}) FTIR spectrum (490–4000 cm^{-1}) of KH*I having a peak assigned to $H^-(\frac{1}{4})$ that matched the predicted frequencies of ortho- and para-$H_2(\frac{1}{4})$ and by the observation of the 1943/2012 cm^{-1}-peak-intensity ratio of 3:1 in the high resolution (0.5 cm^{-1}) FTIR spectrum (1875–2060 cm^{-1}) of KH*I which is characteristic of ortho–para hydrogen splitting wherein the ortho–para splitting of 69 cm^{-1} matched that predicted. As reported in Section 3.1.4, the same energy spacing of 0.24 eV was observed from spectroscopy of electron-beam-excited KH*Cl having a −4.4 ppm NMR peak assigned to $H^-(\frac{1}{4})$ (Section 3.1.2). The results of this paper support past results of rt-plasma formation with intense hydrogen

Lyman emission, a stationary inverted Lyman population, excessive afterglow duration, highly energetic hydrogen atoms, characteristic alkali-ion emission due to catalysis, predicted novel spectral lines, and power generation beyond any conventional chemistry that matched predictions for an energetic catalytic reaction of atomic hydrogen to form more stable hydride ions and hydrogen molecules designated $H^-(1/p)$ and $H_2(1/p)$ [13].

3.2.5. Applications

In addition to the results presented in Sections 3.1.2–3.1.4 and 3.2.3, novel alkaline and alkaline earth hydride and halidohydrides were previously identified by large distinct upfield ^1H NMR resonances compared to the NMR peaks of the corresponding ordinary hydrides [13,15,29,31–33]. Using a number of analytical techniques such as XPS and time-of-flight-secondary-mass-spectroscopy (ToF-SIMS) as well as NMR, the hydrogen content was assigned to $H^-(1/p)$, novel high-binding-energy hydride ions in stable fractional principal quantum states [9,13,31–33]. Upfield shifts of the novel hydride compounds matched those predicted for $H^-(\frac{1}{2})$ and $H^-(\frac{1}{4})$ (Eq. (17)). Novel spectral emission from $H^-(\frac{1}{2})$ and $H^-(\frac{1}{4})$, the predicted products from the potassium catalyst reaction and the supporting results of (1) the formation of a hydrogen plasma with intense extreme ultraviolet (EUV) emission at low temperatures (e.g. $\approx 10^3$ K) and an extraordinary low field strength of about 1–2 V/cm [9–16,21–25] or without an electric field or power input other than thermal [13,14] from atomic hydrogen and certain atomized elements or certain gaseous ions that serve as catalysts, (2) a high positive net enthalpy of reaction [13,29], (3) characteristic predicted catalyst emission [21,22,24,25], (4) $\sim$ 15 eV Doppler broadening of the Balmer lines [13,24,25], and (5) inversion of the Lyman lines [24,25] have also been reported previously.

Hydride ions with increased binding energies form novel compounds with potential for future applications in many industries including chemical, electronics, computer, military, energy, and aerospace in the form of products such as battery materials, propellants, solid fuels, surface coatings, structural materials, and chemical processes. As shown in Table 2, the binding energies given by Eq. (15) go through a maximum stability at $p = 16$ and decrease in stability such that $p = 24$ corresponds to the last stable ion of the series. Applications are anticipated based on this range of stability. Significant applications also exist for the corresponding molecular species $H_2(1/p)$.

(i) *High voltage battery*: Hydride ions having extraordinary binding energies may stabilize a cation M^{x+} in an extraordinarily high oxidation state such as +2 in the case of lithium. Thus, these hydride ions may be used as the basis of a high voltage battery of a rocking-chair design wherein the hydride ion moves back and forth between the cathode and anode half cells during discharge and charge cycles. Exemplary reactions for a cation M^{x+} are

Cathode reaction:

$$MH_x + e^- \rightarrow MH_{x-1} + H^-. \tag{24}$$

Anode reaction:

$$MH_{x-2} + H^- \rightarrow MH_{x-1} + e^-. \tag{25}$$

Overall reaction:

$$MH_x + MH_{x-2} \rightarrow 2MH_{x-1}. \tag{26}$$

(ii) *Energetic propellant*: The reaction to form $H_2(1/p)$ from a hydride compound $M^+H^-(1/p)$ containing $H^-(1/p)$ where M^+ is a metal ion such as Li^+ and $p \approx 24$ represents a potentially very energetic reaction. In the application of $M^+H^-(1/p)$ as a solid, liquid, or gaseous rocket fuel, rocket propellant power may be provided by reaction of $M^+H^-(1/p)$ with a proton to form $H_2(1/p)$ or by the thermal decomposition of $M^+H^-(1/p)$ to form $H_2(1/p)$.[1] The total energy of $H_2(1/p)$ and $H^-(1/p)$ are given by Eqs. (5) and (15), respectively. Using $32p^2$ eV as an estimate of the total energy of $H_2(1/p)$ and the total energy of $H(1/p)$ given by Eqs. (2a) and (2c) as an estimate of total energy of $H^-(1/p)$, the energy balance of the proton reaction is

$$M^+H^-(1/p) + H^+X^- \rightarrow H_2(1/p) + MX + p^2(32 - 13.6)\,\text{eV}. \tag{27}$$

The energy of the decomposition reaction is

$$2M^+H^-(1/p) \xrightarrow{\Delta} H_2(1/p) + 2M + p^2(32 - 2 \cdot 13.6)\,\text{eV}. \tag{28}$$

Very high energy balances are possible as p approaches the limit for a stable hydride ion at 24. In the case of $H^-(\frac{1}{24})$, the energy balances for Eqs. (27) and (28) are truly unconventional, 10 and 2.7 keV, respectively. The mass of the reactants of Eqs. (27) and (28) may be comparable to those of hydrogen combustion that releases 1.48 eV per hydrogen atom; thus, energies of about 7000 and 2000 times that of the conventional hydrogen–oxygen reaction, respectively, are expected. Thus, a $H^-(\frac{1}{24})$-based propellant may be transformational especially given the logarithmic dependence on fuel-weight to lift in the rocketry equation [62].

(iii) *UV Laser*: The existence of excited vibration–rotational levels of $H_2(1/p)$ in gas phase (Section 3.1.1) and from these molecules trapped in a crystalline lattice (Section 3.1.3) presents the possibility of a laser using a transition from a vibration–rotational level to another lower-energy-level other than one with a significant Boltzmann population at the cell neutral-gas temperature (e.g. one with both υ and $J = 0$). A laser may be realized using cavities and mirrors that are appropriate for the desired wavelength similar to those of current lasers based on molecular vibration–rotational levels such as the CO_2 laser. However, an advantage exists to produce laser light at much shorter wavelengths. The current results anticipate a laser based on vibration–rotational levels of $H_2(\frac{1}{4})$ that lases in the UV. Such lasers have significant application in photolithography.

[1] The helium–hydrogen microwave plasma contains H^+ which favors the reaction product $H_2(1/p)$ over $H^-(1/p)$ due to the highly exothermic reaction of Eq. (27) wherein X^- is a plasma electron or ordinary hydride ion. $HeH(\frac{1}{2})$ is also not favored due to the highly exothermic reaction to form $H_2(\frac{1}{2})$.

Table 2
The ionization energy of the hydride ion $H^-(1/p)$ as a function of p

Hydride ion	r_1 (a_0)[a]	Calculated ionization energy[b] (eV)	Calculated wavelength (nm)
$H^-(n=1)$	1.8660	0.7542	1644
$H^-(n=\frac{1}{2})$	0.9330	3.047	406.9
$H^-(n=\frac{1}{3})$	0.6220	6.610	187.6
$H^-(n=\frac{1}{4})$	0.4665	11.23	110.4
$H^-(n=\frac{1}{5})$	0.3732	16.70	74.23
$H^-(n=\frac{1}{6})$	0.3110	22.81	54.35
$H^-(n=\frac{1}{7})$	0.2666	29.34	42.25
$H^-(n=\frac{1}{8})$	0.2333	36.09	34.46
$H^-(n=\frac{1}{9})$	0.2073	42.84	28.94
$H^-(n=\frac{1}{10})$	0.1866	49.38	25.11
$H^-(n=\frac{1}{11})$	0.1696	55.50	22.34
$H^-(n=\frac{1}{12})$	0.1555	60.98	20.33
$H^-(n=\frac{1}{13})$	0.1435	65.63	18.89
$H^-(n=\frac{1}{14})$	0.1333	69.22	17.91
$H^-(n=\frac{1}{15})$	0.1244	71.55	17.33
$H^-(n=\frac{1}{16})$	0.1166	72.40	17.12
$H^-(n=\frac{1}{17})$	0.1098	71.56	17.33
$H^-(n=\frac{1}{18})$	0.1037	68.83	18.01
$H^-(n=\frac{1}{19})$	0.0982	63.98	19.38
$H^-(n=\frac{1}{20})$	0.0933	56.81	21.82
$H^-(n=\frac{1}{21})$	0.0889	47.11	26.32
$H^-(n=\frac{1}{22})$	0.0848	34.66	35.76
$H^-(n=\frac{1}{23})$	0.0811	19.26	64.36
$H^-(n=\frac{1}{24})$	0.0778	0.6945	1785
$H^-(n=\frac{1}{25})$		Not stable	

[a]From Eq. (15) where a_0 is the Bohr radius.
[b]From Eq. (15).

Lithography, the technique for manufacturing microelectronics semiconductor devices such as processors and memory chips, presently uses deep UV radiation at 193 nm from the ArF excimer laser. Future sources are F_2 lasers at 157 nm and perhaps H_2 lasers at 127 nm. Advancements in light sources are required in order to achieve the steady reduction in the size of integrated circuits. Only a free electron laser (FEL) with a minimum beam energy of 500 MeV appears suitable as a light source for the Next Generation Lithography (NGL) based on EUV lithography (13.5 nm) [63,64]. With our discovery, the opportunity may exist to replace a FEL that occupies the size of a large building with a table-top laser for the desired 10–14 nm range based on vibration–rotational-state inversion of $H_2(\frac{1}{13})$.

4. Conclusion

In this study we made specific theoretical predictions and tested them with standard, easily interpretable experiments. The results show that the possibility that a novel reaction of atomic hydrogen that uses certain catalysts such as He^+, Ar^+, and K may be a clean new energy source is supported by spectroscopic, chemical, and thermal data. For example, we report the discovery of new states of hydrogen formed in a catalytic plasma reaction. The atomic states $H(1/p)$ were identified previously [1–3] by the spectroscopic observation of emission lines occurring at energies that are an extension of the Rydberg series to lower states. A corresponding molecule, $H_2(\frac{1}{4})$, was identified by vibrational–rotational series emission from an electron-beam-maintained plasma of argon–hydrogen that established an internuclear distance of $\frac{1}{4}$ that of the ordinary hydrogen species. This identification was confirmed in independent experiments. For example, the predicted frequencies of ortho- and para-$H_2(\frac{1}{4})$ were observed at 1943 cm^{-1} and 2012 cm^{-1} in the high resolution FTIR spectrum of KH*I having a −4.6 ppm NMR peak assigned to $H^-(\frac{1}{4})$. The 1943/2012 cm^{-1}-intensity ratio matched the characteristic ortho-to-para-peak-intensity ratio of 3:1, and the ortho–para splitting of 69 cm^{-1} matched that predicted. KH*Cl having $H^-(\frac{1}{4})$ by NMR was incident to the 12.5 keV electron-beam which excited similar emission of interstitial $H_2(\frac{1}{4})$ as observed in the argon–hydrogen plasma.

The molecular hydrogen gas product was isolated by liquefaction at liquid nitrogen temperature and by decomposition of compounds previously found to contain the corresponding

hydride ions $H^-(1/p)$ [7,13,31–33]. Singlet peaks upfield of H_2 with a predicted integer spacing of 0.64 ppm at 3.47, 3.02, 2.18, 1.25, 0.85, and 0.22 ppm identified as the consecutive series $H_2(\frac{1}{2})$, $H_2(\frac{1}{3})$, $H_2(\frac{1}{4})$, $H_2(\frac{1}{5})$, $H_2(\frac{1}{6})$, and $H_2(\frac{1}{7})$ and $H_2(\frac{1}{10})$ at −1.8 ppm provides powerful confirmation of the existence of $H_2(1/p)$. Furthermore, the ^{1}H NMR spectra of gases from the thermal decomposition of KH*I matched those of LN-condensable hydrogen which provides strong support that compounds such as KH*I contain hydride ions $H^-(1/p)$ in the same fractional quantum state p as the observed $H_2(1/p)$. Observational agreement with predicted positions of upfield-shifted ^{1}H MAS NMR peaks (Eq. (17)) of the compounds, catalyst reactions, and spectroscopic data supports this conclusion. On this basis, possibilities for advanced technologies are considered.

It was reported previously that stationary inverted H populations were formed by using certain catalysts in hydrogen plasmas, and novel processes and hydride products with significant commercial potential were characterized by EUV and visible spectroscopy, NMR, ToF-SIMS, and XPS. Very high (> 100 eV) H energies and substantial excess thermal energy were observed [17,18]. Using water bath calorimetry in this study, excess power was observed from the helium–hydrogen plasma compared to control krypton plasma. For example, for an input of 41.9 W, the total plasma power of the helium–hydrogen plasma measured by water bath calorimetry was 62.1 W corresponding to 20.2 W of excess power in 3 cm^3. The excess power density and energy balance were high, 6.7 W/cm^3 and -5.4×10^4 kJ/mole H_2 (280 eV/H atom), respectively. The reaction of hydrogen to form water which releases −241.8 kJ/mole H_2 (1.48 eV/H atom) is about 200 times less than that observed.

The results indicate that a new power source based on the catalysis of atomic hydrogen is not only possible, but it may be competitive with gas-turbine combustion. Furthermore, since the identified $H_2(1/p)$ byproduct is stable and lighter-than-air, it cannot accumulate in the Earth's atmosphere. The environmental impact of handling fossil fuels and managing the pollution of air, water, and ground caused by the ash generated by fossil fuels or the radioactive waste from a nuclear plant may be eliminated.

Based on their stability characteristics, advanced hydride technologies are indicated. Hydride ions $H^-(1/p)$ having extraordinary binding energies may stabilize a cation M^{x+} in an extraordinarily high oxidation state as the basis of a high voltage battery. And, a rocketry propellant based on $H^-(\frac{1}{24})$ to $H_2(\frac{1}{24})$ may be possible with an energy release so large that it may be transformational. Significant applications also exist for the corresponding molecular species $H_2(1/p)$. The results of this study indicate that excited vibration–rotational levels of $H_2(\frac{1}{4})$ could be the basis of a UV laser that could significantly advance photolithography.

Acknowledgments

Special thanks to D.E. Murnick and M. Salvermoser of Rutgers University for assistance with the 12.5 keV electron gun. D.C. Harris, Naval Air Warfare Center Weapons Division, Naval Air Warfare Center, China Lake, CA, is acknowledged for suggesting the method of identifying $H_2(1/p)$ by ^{1}H NMR using $CDCl_3$ solvent. D.C. Harris and L. Merwin are acknowledged for preparing and analyzing a KH*I NMR sample.

References

[1] Mills RL, Ray P. Extreme ultraviolet spectroscopy of helium-hydrogen plasma. J Phys D Appl Phys 2003;36:1535–42.
[2] Mills RL, Ray P, Dhandapani B, Nansteel M, Chen X, He J. New power source from fractional quantum energy levels of atomic hydrogen that surpasses internal combustion. J Mol Struct 2002;643(1–3):43–54.
[3] Mills RL, Ray P. Spectral emission of fractional quantum energy levels of atomic hydrogen from a helium-hydrogen plasma and the implications for dark matter. Int J Hydrogen Energy 2002;27(3):301–22.
[4] Bruch R, Altick PL, Trabert E, Heckmann PH. High-resolution EUV satellite spectra of doubly excited He I (nln′l′), n = 2 to 5. J Phys B At Mol Phys 1984;17:L655–60.
[5] Sidgwick NV. The chemical elements and their compounds Oxford: Clarendon Press; vol. I, 1950 p. 17.
[6] Lamb MD. Luminescence spectroscopy. London: Academic Press; 1978 p. 68.
[7] Mills RL. The grand unified theory of classical quantum mechanics, April (2007) edition posted at ⟨www.blacklightpower.com⟩.
[8] Mills RL. The nature of the chemical bond revisited and an alternative Maxwellian approach. Phys. Essays 2004;17:342–89.
[9] Mills RL, Dong J, Lu Y. Observation of extreme ultraviolet hydrogen emission from incandescently heated hydrogen gas with certain catalysts. Int J Hydrogen Energy 2000;25:919–43.
[10] Mills RL, Nansteel M, Ray P. Argon-hydrogen-strontium discharge light source. IEEE Trans Plasma Sci 2002;30(2):639–53.
[11] Mills RL, Nansteel M, Ray P. Bright hydrogen-light source due to a resonant energy transfer with strontium and argon ions. New J Phys 2002;4 70.1–70.28.
[12] Mills RL, Nansteel M, Ray P. Excessively bright hydrogen-strontium plasma light source due to energy resonance of strontium with hydrogen. J Plasma Phys 2003;69:131–58.
[13] Mills RL, Ray P, Dhandapani B, Good W, Jansson P, Nansteel M. et al. Spectroscopic and NMR identification of novel hydride ions in fractional quantum energy states formed by an exothermic reaction of atomic hydrogen with certain catalysts. Eur Phys J Appl Phys 2004;28:83–104.
[14] Conrads H, Mills RL, Wrubel T. Emission in the deep vacuum ultraviolet from a plasma formed by incandescently heating hydrogen gas with trace amounts of potassium carbonate. Plasma Sources Sci Technol 2003;12:389–95.
[15] Mills RL, He J, Nansteel M, Dhandapani B. Catalysis of atomic hydrogen to new hydrides as a new power source, in press.
[16] Mills RL, Nansteel M, He J, Dhandapani B. Low-voltage EUV and visible light source due to catalysis of atomic hydrogen, submitted for publication.
[17] Mills RL, Ray P, Dhandapani B, Mayo RM, He J. Comparison of excessive Balmer α line broadening of glow discharge and microwave hydrogen plasmas with certain catalysts. J Appl Phys 2002;92(12): 7008–22.
[18] Mills RL, Ray P, Dhandapani B, He J. Comparison of excessive Balmer α line broadening of inductively and capacitively coupled RF, microwave, and glow discharge hydrogen plasmas with certain catalysts. IEEE Trans Plasma Sci 2003;31(3):338–55.
[19] Mills RL, Ray P. Substantial changes in the characteristics of a microwave plasma due to combining argon and hydrogen. New J Phys 2002;4 22.1–22.17.
[20] Phillips J, Chen C-K, Shiina T. Evidence of catalytic production of hot atomic hydrogen in RF generated hydrogen/helium plasma, submitted for publication. Available at http://arxiv.org/ftp/physics/papers/0509/0509127.pdf.

[21] Mills RL, Ray P. A comprehensive study of spectra of the bound-free hyperfine levels of novel hydride ion $H^-(\frac{1}{2})$, hydrogen, nitrogen, and air. Int J Hydrogen Energy 2003;28(8):825–71.
[22] Mills RL, Ray P. Spectroscopic identification of a novel catalytic reaction of potassium and atomic hydrogen and the hydride ion product. Int J Hydrogen Energy 2002;27(2):183–92.
[23] Mills RL. Spectroscopic identification of a novel catalytic reaction of atomic hydrogen and the hydride ion product. Int J Hydrogen Energy 2001;26(10):1041–58.
[24] Mills RL, Ray P, Mayo RM. CW HI laser based on a stationary inverted Lyman population formed from incandescently heated hydrogen gas with certain group I catalysts. IEEE Trans Plasma Sci 2003;31(2):236–47.
[25] Mills RL, Ray P. Stationary inverted Lyman population formed from incandescently heated hydrogen gas with certain catalysts. J Phys D 2003;36:1504–9.
[26] Mills RL, Ray P, Mayo RM. The potential for a hydrogen water-plasma laser. Appl Phys Lett 2003;82(11):1679–81.
[27] Phillips J, Mills RL, Chen X. Water bath calorimetric study of excess heat in 'resonance transfer' plasmas. J Appl Phys 2004;96(6):3095–102.
[28] Mills RL, Chen X, Ray P, He J, Dhandapani B. Plasma power source based on a catalytic reaction of atomic hydrogen measured by water bath calorimetry. Thermochim Acta 2003;406(1–2):35–53.
[29] Mills RL, He J, Chang Z, Good W, Lu Y, Dhandapani B. Catalysis of atomic hydrogen to novel hydrides as a new power source, Prepr. Pap.-Am. Chem. Soc., Div. Fuel Chem. 2005;50(2).
[30] Mills RL, Lu Y, Nansteel M, He J, Voigt A, Dhandapani B. Energetic catalyst-hydrogen plasma reaction as a potential new energy source. Division of Fuel Chemistry, Session: Chemistry of Solid, Liquid, and Gaseous Fuels, 227th American Chemical Society National Meeting, March 28–April 1, 2004, Anaheim, CA.
[31] Mills RL, Dhandapani B, Nansteel M, He J, Shannon T, Echezuria A. Synthesis and characterization of novel hydride compounds. Int J Hydrogen Energy 2001;26(4):339–67.
[32] Mills RL, Dhandapani B, Greenig N, He J. Synthesis and characterization of potassium iodo hydride. Int J Hydrogen Energy 2000;25(12): 1185–203.
[33] Mills RL, Dhandapani B, Nansteel M, He J, Voigt A. Identification of compounds containing novel hydride ions by nuclear magnetic resonance spectroscopy. Int J Hydrogen Energy 2001;26(9):965–79.
[34] Lide DR. CRC handbook of chemistry and physics. 79th ed., Boca Raton: CRC Press; 1998 1999. p. 10–175.
[35] Beutler H. Die dissoziationswarme des wasserstoffmolekuls H_2, aus einem neuen ultravioletten resonanzbandenzug bestimmt. Z Physical Chem 1934;27B:287–302.
[36] Herzberg G, Howe LL. The Lyman bands of molecular hydrogen. Can J Phys 1959;37:636–59.
[37] Atkins PW. Physical chemistry. 2nd ed., San Francisco: W.H. Freeman; 1982 p. 589.
[38] Karplus M, Porter RN. Atoms and molecules an introduction for students of physical chemistry. Menlo Park: The Benjamin/Cummings Publishing Company; 1970 p. 447–84.
[39] Raynes WT, Panteli N. The extraction of a nuclear magnetic shielding function for the H_2 molecule from spin-rotation and isotope shift data. Mol Phys 1983;48(3):439–49.
[40] Sundholm D, Gauss J, Ahlrichs R. The electron correlation contribution to the nuclear magnetic shielding tensor of the hydrogen molecule. Chem Phys Lett 1995;243:264–8.
[41] Raynes WT, Panteli N. The nuclear spin–spin coupling in the hydrogen molecule: its equilibrium valve and bond-length dependence. Chem Phys Lett 1983;94:558–60.
[42] Stavola M, Chen EE, Fowler WB, Shi GA. Interstitial H_2 in Si: are all problems solved?. Phys B 2003; 340–2 58–66.
[43] Lavrov EV, Weber J. Ortho and para interstitial H_2 in silicon. Phys Rev Lett 2002;89(21) 215501-1–215501-4.
[44] Stavola M, Chen EE, Fowler WB, Zhou JA. Rotation of molecular hydrogen in Si: unambiguous identification of ortho-H_2 and para-D_2. Phys Rev Lett 2002;88(24) 245503-1–245503-4.
[45] Stavola M, Chen EE, Fowler WB, Walters P. Key to understanding interstitial H_2 in Si. Phys Rev Lett 2002;88(10) 105507-1–105507-4.
[46] Leitch AWR, Alex V, Weber J. Raman spectroscopy of hydrogen molecules in crystalline silicon. Phys Rev Lett 1998;81(2):421–4.
[47] Lykke KR, Murray KK, Lineberger WC. Threshold photodetachment of H^-. Phys Rev A 1991;43(11):6104–7.
[48] Abeles F, editors. Optical properties of solids; 1972. p. 725.
[49] Wieser J, Murnick DE, Ulrich A, Higgins HA, Liddle A, Brown WL. Vacuum ultraviolet rare gas excimer light source. Rev Sci Instrum 1997;68(3):1360–4.
[50] Ulrich A, Wieser J, Murnick DE. Excimer formation using low energy electron beam excitation second international conference on atomic and molecular pulsed lasers. Proc SPIE 1998;3403:300–7.
[51] Shuaibov AK, Dashchenko AI, Shevera IV. Stationary radiator in the 130–190 nm range based on water vapour plasma. Quant Electron 2001;31(6):547–8.
[52] Shuaibov AK, Shimon LL, Dashchenko AI, Shevera IV. Optical characteristics of a glow discharge in a He/H_2O mixture. Plasma Phys Rep 2001;27(10):897–900.
[53] NIST Atomic Spectra Database, ⟨www.physics.nist.gov/cgi-bin/AtData/display.ksh⟩.
[54] Baldridge KK, Siegel JS. Correlation of empirical δ(TMS) and absolute NMR chemical shifts predicted by ab initio computations. J Phys Chem A 1999;103:4038–42.
[55] Mason J, editor. Multinuclear NMR. New York: Plenum Press; 1987 [chapter 3].
[56] von Engel A. Ionized gases. New York: American Institute of Physics Press; 1965 p. 62–4.
[57] Lide DR. CRC handbook of chemistry and physics. 76th ed., Boca Raton: CRC Press; 1995–6 p. 6–66 and p. 6–140.
[58] Levine IN. Physical chemistry. New York: McGraw-Hill Book Company; 1978 p. 174–5.
[59] Gottlieb HE, Kotlyar V, Nudelman A. NMR chemical shifts of common laboratory solvents as trace impurities. J Org Chem 1997;62:7512–5.
[60] Suarez C, Nicholas EJ, Bowman M. Gas-phase dynamic NMR study of the internal rotation in N-trifluoroacetlypyrrolidine. J Phys Chem A 2003;107:3024–9.
[61] Suarez C. Gas-phase NMR spectroscopy. Chem Educator 1998;3(2).
[62] Fowles GR. Analytical mechanics. 3rd ed., New York: Holt, Rinehart, and Winston; 1977 p. 182–4.
[63] Bjorkholm JE. EUV lithography—the successor to optical lithography?. Intel Technol J 1998;Q3:1–8.
[64] Hesch K, Pellegrin E, Rossmanith R, Steininger R, Saile V, Wust J, et al. Extreme ultraviolet (EUV) sources based on synchrotron radiation. Proceedings of the 2001 particle accelerator conference, June 18–22, 2001, Chicago. p. 654–6.